NTNU
Norwegian University of
Science and Technology

A Model for the Mixing of Black Carbon Aerosols and Mineral Dust Particles in the Atmosphere

Simen Berntsen

Master of Science in Physics and Mathematics
Submission date: June 2016
Supervisor: Alex Hansen, IFY

Norwegian University of Science and Technology
Department of Physics

”big whirls have little whirls that feed on their velocity, and little whirls have lesser whirls and so on to viscosity”

Lewis Fry Richardson, 1922

Abstract

The process when freshly emitted black carbon particles are forming clusters and the mixing of these black carbon clusters and mineral dust particles has been simulated for a two-dimensional system. This has been done by combining diffusion-limited cluster aggregation and multifractal turbulent velocity fields. A simple model where the mineral dust particles drive the deposition of black carbon has been developed and investigated, suited for quantifying the deposition of black carbon aerosols in dry, desert-like areas such as Sahara or the Arabian peninsula. This is of interest as it is assumed that the lifetime of black carbon particles in the soil of these areas are very long. The deposition of black carbon may change the albedo of the surface of the Earth, which may effect both local weather and the climate. The results from the model, although uncertain, indicate that the lifetime of black carbon in the atmosphere with respect to uptake on larger dust aerosols is short enough to allow a substantial fraction of the BC emitted (mostly from flaring from oil/gas extraction) to be deposited in the high albedo desert regions where emissions occur.

Sammendrag

Prosessen der nyutsluppede svarte karbonpartikler danner klynger, og blandingen av disse svarte karbonklyngene og mineralstøv har blitt simulert for et todimensjonalt system. Dette har blitt gjort ved å kombinere diffusjonsbegrenset klyngeaggregering og multifraktale turbulente hastighetsfelt. En enkel model hvor mineralstøvet styrer deponeringen av svart karbon har blitt utviklet og studert. Modellen er egnet for å kvantisere deponeringen av svart karbon i tørre ørkenområder som Sahara og Den arabiske halvøy. Dette er interessant fordi det antas at svart karbon har en svært lang levetid på jordoverflaten i ørkenområder. Deponeringen av svart karbon kan endre albedoen til overflaten, noe som kan påvirke både vær og klima. Resultatene fra modellen, om enn usikre, indikerer at levetiden til svart karbon i atmosfæren relatert til sammenslåing med større støvpartikler er kort nok til at en stor del av utsluppede karbonet (fra olje/gassfakler) vil bli deponert i disse områdene med høy albedo hvor utslippene foregår.

Preface

This thesis is the final work of a Masters degree in Applied Physics at the Norwegian University of Science and Technology. First I would like to thank my supervisor Prof. Alex Hansen and his Ph.D. student Morten Vassvik for all guidance throughout this thesis. I would also like to thank Arve Kylling at NILU for providing me with some background/motivation for my work. A big thanks to all my friends and fellow students for making my time as a student every bit as enjoyable as it should be. Finally I would like to thank my parents, my better half Thale, and my family.

Simen Berntsen
Trondheim, Norway
June 2016

Table of Contents

List of Tables

List of Figures

Abbreviations

BC	=	Black Carbon
DLA	=	Diffusion Limited Aggregation
DLCA	=	Diffusion Limited Cluster Aggregation
CO_2	=	Carbon Dioxide
K41-theory	=	Kolmogorovs statistical theory of tubulence from 1941
OD	=	Open Domain
PBC	=	Periodic Boundary Conditions
CPU	=	Central Processing Unit
AABB	=	Axis Aligned Bounding Box
RAM	=	Random Access Memory
PM_{10}	=	Particulate Matter $< 10\ \mu\mathrm{m}$

Chapter 1

Introduction

Black carbon (BC) aerosols are formed from incomplete combustion of fossil fuels and biomass. Surplus carbon clump together to form clusters, which are then released into the atmosphere. An example of this is shown in Figure 1.1. These BC aerosols appear to contribute significantly to both climate change and local weather effects, and it is of great interest to understand how the aerosols cause these effects. A lot of research has been done on this, and there is general consensus that some of the effects are well understood, while others are still quite uncertain.

BC may for instance affect the climate simply by being dark aerosols (Haywood and Shine (1995)), as the aerosols absorbs radiation and heats the atmosphere (direct effect). The optical properties of pure BC cluster aerosols (Liousse et al. (1993)) have been studied as a result of this, as well as hybrids where BC clusters are mixed with other aerosols, for instance by Clarke et al. (2004). The BC aerosols may also have an influence on the cloud cover, resulting in a ”semi-direct” effect on heating (Koch and Del Genio (2010)). Lastly, in the atmosphere, BC may act as cloud condensation nuclei in warm clouds, which increase brightness and reduce precipitation (Bond et al. (2013)) A similar effect has been found in cold or mixed-phase clouds, although this is not understood as well as for warm clouds (Bond et al. (2013)).

Another key property of the BC aerosols is that they may originate from man made emissions, meaning a large part of their climate effects are by extension caused by humans (are anthropogenic). They are thus fundamentally different from for instance mineral dust aerosols in the sense that they represent a controllable climatological factor. An additional consequence of this is that once the aerosols are deposited, they might have a strong effect on the albedo (reflection coefficient) of the surface of the Earth as the aerosols did not originate from there. The aerosols can be deposited on high reflectivity areas, for instance covered by snow/ice, to darken the surface and decrease the albedo (Hansen and Nazarenko (2004)). This effect may occur for any aerosol deposited with a reflectivity lower than the surface it is deposited on, but due to the BC aerosols being black, they will in general have a lower reflectivity than any surface in nature they may be deposited on.

One is however most interested in the areas where the change in albedo is the greatest, because of the resulting change in energy absorption. Following this argument, one has traditionally studied the effect on snow/ice, as an increase in absorption will increase melting rate, giving a positive feedback as darker ground is uncovered (Flanner et al. (2009)). Recent studies (Sand et al. (2015)) suggest that emission of BC from flaring (see Figure 1.1 for an example, although not in Russia) in oil and gas fields in Northwest Russia has the greatest climatological effect per unit emission on the Arctic region.

Figure 1.1: Photo of a gas flare in Thailand. The photo is taken from Krittaya (2007). Notice how the BC form a seemingly black smoke due to the very high concentration of BC released in the plume.

In analogy to this, one would like to investigate the effect of BC aerosols from oil/natural gas fields in subtropical desert areas with relatively high albedo and high insolation (power received on Earth per unit area on a horizontal surface). Although one does not get a fundamental change in the surface properties, these areas are of particular interest due to their emissions related to extraction of fossil fuels, high annual insolation, low precipitation, very slow chemical or biological processes removing the deposited BC. Previous model studies have not predicted significant deposition of BC particles in these areas due to the low deposition velocity of the small BC particles and lack of precipitation. However, recent observations (Scarnato et al. (2015)) show that BC particles can coagulate with larger mineral dust particles and thus be deposited at a much faster rate. The hypothesis is that a high density of mineral dust in the lower atmosphere can significantly increase the deposition rate of BC and cause a long-term warming of the climate system.

It is assumed that due to the previously mentioned factors, the lifetime for the BC particles on the ground may be very long (as opposed to in the case of snow/ice where the BC are washed away/mixed with the soil after the melting has occurred). In a shorter time frame, the reduced albedo increases the absorption on the earths surface, and subsequently heats the lower layer of air in the atmosphere. Due to the stably stratified atmosphere in the high-pressure regions over the subtropical dessert regions, this hot, dry air is not transported from the surface very efficiently, which results in heat waves during summertime. It is suspected that the reduction of the albedo in these areas will further enhance this.

A first step in quantifying the possible climate impacts is to estimate the deposition rates of BC. In order to estimate this for the previously described areas, one is interested in both transport and agglomeration rate of the BC particles. Agglomeration rate because pure BC clusters will have a negligible fall velocity (Flagan and Seinfeld (1988)), and transport rate because it will determine how far from the source these clusters can reach before they are deposited. This thesis builds on the work done by Berntsen (2015b) where numerical methods for generating the BC clusters were investigated. In particular the diffusion-limited aggregation (DLA) method proposed by Witten and Sander (1981) was investigated, and customized to diffusion-limited cluster aggregation (DLCA) as described by Meakin (1983). The results were analysed using the framework of Vicsek and Family (1984) and the results of Meakin et al. (1985).

In the continuation presented in this thesis, the agglomeration rate is investigated, under the hypothesis that the mechanism driving deposition is the mixing of BC clusters with heavier mineral dust particles in the atmosphere. The aims of the work have been to:

- Understand the turbulent mixing of particles also affected by diffusion.
- Develop a model for simulating this mixing in a dynamic turbulent velocity field.
- Investigate the deposition rate when using this model.

To accomplish this, an improvement on the algorithm used by Berntsen (2015b) was implemented. To make the simulations as close to the real world one tries to simulate, both open domain (OD) simulations and periodic boundary condition (PBC) simulations were performed. In practice, it is assumed that one has a source of BC particles in a field populated with heavier mineral dust particles, which the BC may attach to. These dust particles will eventually settle due to their non-negligible fall velocity, which is the mechanism assumed to be driving the deposition of the BC clusters. The model that has been developed for simulating this system is

presented and discussed, along with the main physical effects that are included in the model. The results from using this model are presented and analysed, both with respect to the model itself and how suited the model is to simulate the proposed scenario.

All the code used in this project was developed specifically for the purpose, and implemented as a C++ program. It can be found in Berntsen (2015a).

1.1 Motivation

To elaborate on why this is a problem worth studying, a short estimate of the possible impact the emission of BC particles in high-albedo areas can have has been calculated by Kylling (2016) at the Norwegian Institute for Air Research (NILU). As this is unpublished work done to get a rough estimate of the climatological effects this thesis tries to understand, the work will be explained in detail. The author calculates the instantaneous radiative forcing

$$RF = E^{f}_{\text{net}} - E^{bg}_{\text{net}}, \tag{1.1}$$

where E is the irradiance. The superscripts f and bg denote calculations with the forcing agent included and background conditions without the forcing agent, respectively. Furthermore

$$E_{\text{net}} = E^{+} - E^{-} = E^{+}_{\text{solar}} + E^{+}_{\text{thermal}} - E^{-}_{\text{solar}} + E^{-}_{\text{thermal}}, \tag{1.2}$$

where E^{+} and E^{-} denotes upwelling and downwelling respectively, at a given level of the atmosphere. The author uses the `uvspec` model from the `libRadtran` software package from Mayer and Kylling (2005) to calculate the solar and thermal up- and downwelling irradiances. Moreover, the radiative transfer equation was solved using an improved `DISORT` solver (Stamnes et al. (1988), Buras et al. (2011)) in pseudo spectral geometry (Dahlback and Stamnes (1991)).

The assumptions for the radiative forcing simulations are as follows; that there are no clouds, and a decrease in land surface albedo of 0.5%. This surface albedo number is naively taken by the author from Marks and King (2013), a study of BC in arctic sea ice where it was found that BC decrease the surface albedo at 500 nm to between 98.7% and 99.7% of the original value. Based on this it was assumed that BC reduce the desert albedo by up to 99.5 % of its original value. The simulated scenario is the best case for insolation, meaning conditions were taken to maximize the radiative forcing. That means that the simulated time of day was noon, during the middle of summer (June 15th). The results are remarkable, and they indicate that the potential effect of a change in surface albedo in dessert areas is dramatic. In these conditions chosen to maximize the radiative forcing, the author finds that the radiative forcing may be increased by between 1 and 2.5 W m^{-2} in the Sahara, depending on the location. The results can be found in Figure 1.2.

To put this in context, one can compare the numbers from Kylling (2016) to the estimated global mean radiative forcing of the increase in the main anthropogenic greenhouse gas carbon dioxide (CO_2) since pre-industrial times of about 1.7 W m^{-2} (Forster et al. (2007) and Stocker (2014)). Although the numbers in Figure 1.2 are for a limited area, it is clear that simply perturbing the albedo of the surface by as little as 0.5% yields a change in radiative forcing which could give a non-negligible contribution to anthropogenic radiative forcing of climate. It does therefore seem highly interesting to pursue a better understanding of the effects that may change the surface albedo of high-insolation areas.

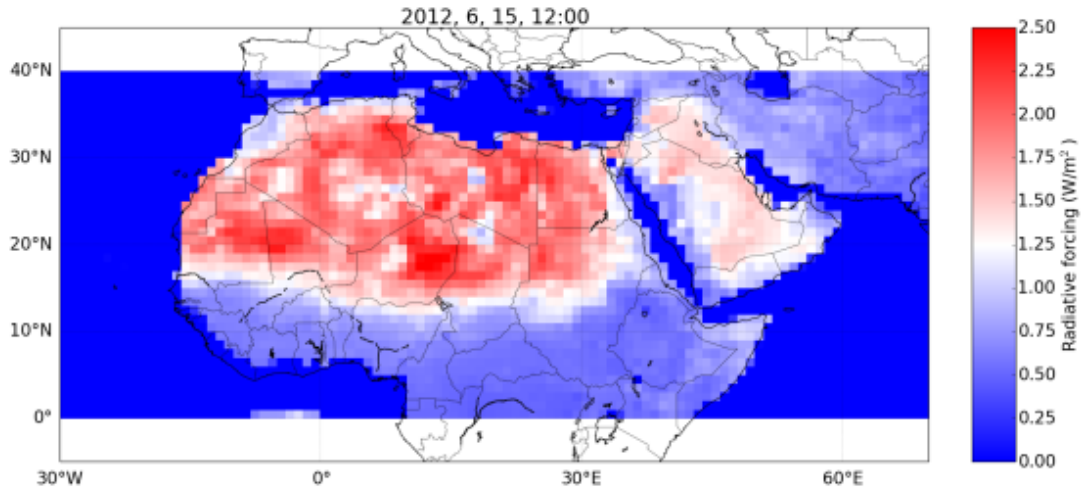

Figure 1.2: Simulated radiative forcing due to a decrease of surface albedo of 0.5%. The figure is taken with permission from Kylling (2016) (private communication).

Chapter 2

Theory

In this chapter the most relevant theory will be discussed, with some of the most important aspects explained in greater detail. Nevertheless, the majority of this section will not be derivations of the equations used in the work presented later, but rather stating the relevant theory and/or equations, and referring to the original works.

As the work presented takes an algorithmic approach to describing physical systems, the relevant theory is somewhat limited. However, the most important framework utilized for analyzing some of the concepts discussed are fractals. To begin with, the basic notion of fractals are presented, which can be used to analyze clusters formed by DLCA. Furthermore, the concept of multifractals are introduced, which are later in this thesis used to generate dynamic turbulent velocity fields. These velocity fields will have an effect on particle dynamics, so the leading equations used in determining the motion of the particles are presented. Finally the concept of diffusion is discussed in the perspective of random walkers.

2.1 Fractals

Fractals are the natural (physical) phenomenon or a mathematical set characterized by having a repeating pattern over different scales. As a result of this, fractals are also the simplest nontrivial example of scale invariance. The term *fractal* dates back to Mandelbrot (1975), however the concept is believed to have been studied by mathematicians such as Leibniz as early as the 17th century. One of the problems of fractals are that they are hard to define rigorously, and they are usually defined by the gestalt of several features. These features include self-similarity, detailed structures at arbitrary scales, irregularities both locally and globally which are not easily described by Euclidean geometry, and simple and recursive definitions. The feature of self-similarity is rather vague, as it includes everything from exact replication of different scales (deterministic fractals), to objects/sets that are self-similar in the statistical sense. In the following introduction to fractals, most of the topics follow Strogatz (1994).

To further explain some of the key features of fractals, it is thus common to look at an example, and explain the fractal features from there. One of the most studied fractals is the Cantor set shown in Figure 2.1, first proposed by Cantor (1883). The Cantor set is generated by recursively splitting a line segment into three, and removing the middle part.

In light of Figure 2.1, one can easily recognize the self-similarity of the fractal. By looking at the right third of the $l = 2$ level, one is left with a set of lines identical to the $l = 1$ level. In

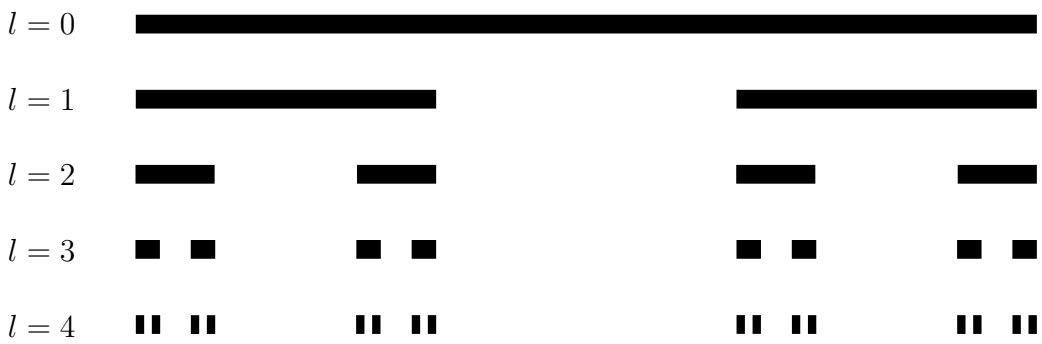

Figure 2.1: The Cantor set. By taking a line segment, dividing it in three equal pieces, one constructs the cantor set. The number l indicates the level of the process, but it should be stressed that this process is done recursively ad infinitum.

general, by zooming in on a level l, one will in the case of the cantor set reconstruct the previous level $l - 1$. This property is key for *deterministic* fractals.

2.1.1 Fractal dimension

Another key property of fractals (and thus also the Cantor set) are that they have non-integer dimensionality. One way of calculating this dimensionality is the so-called box-dimension method. By letting $\mathcal{D}$ be the Euclidean dimension of a space, and the fractal of interest be a subset of this space, one can then cover the fractal with $N(\xi)$ $\mathcal{D}$-dimensional cubes of sides ξ. An illustration is shown in Figure 2.2 of a two-dimension classical set S (being a subset of $\mathcal{D}$, but not a fractal in this case). The amount of boxes required to cover such a two-dimensional structure is $N(\xi) \propto A/\xi^2$, where A is the area of S. In the one-dimensional case the amount would be $N(\xi) \propto L/\xi$, with L being the length of the curve. This is due to a power law

$$N(\xi) \propto \frac{1}{\xi^d}. \tag{2.1}$$

The power law also holds for most fractal sets, where now d is no longer necessarily an integer. This d is called the box-dimension of the set, and can easily be found rewriting (2.1)

$$d = \lim_{\xi \to 0} \frac{\ln N(\xi)}{\ln(1/\xi)}, \tag{2.2}$$

if this limit exists.

2.1.2 Multifractals

Multifractal systems are systems where a single fractal dimension exponent is not enough to describe the dynamics or properties of the system. Although it is a rather new concept, it has a wide range of applications, such as describing fully developed turbulence (Bohr et al. (1998)). The term was first coined by Giorgio Parisi (Frisch and Parisi (1985)), who proposed

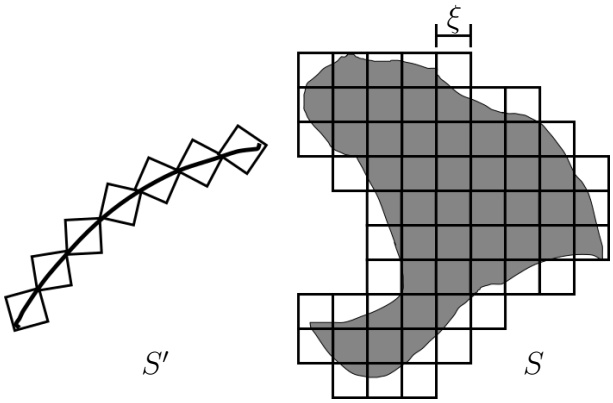

Figure 2.2: Illustration of the box-dimension method for finding the fractal dimension of structures S and S'. Note that both of them are two-dimensional constructs, meaning one requires two-dimensional boxes (squares) in this case. Also keep in mind that in this simple example, S and S' do not represent fractal structures, but are rather simple geometric objects.

that in order to describe the singularities (and thus also the dynamics) of turbulent fields, the common fractals were not sufficient. It is therefore convenient to explain some of the theory of multifractals through the example of fully developed turbulence, and the following short introduction is based on Frisch and Parisi (1985). Before one can follow the arguments of Frisch and Parisi (1985), a brief introduction to the field of turbulence and fluid dynamics is necessary. The equations for determining the motion of fluids are the Navier-Stokes equations

$$\begin{aligned} \partial_t \vec{v} + (\vec{v} \cdot \nabla)\vec{v} &= -\frac{\nabla P}{\rho} + \nu \Delta \vec{v} + \vec{f}, \\ \nabla \vec{v} &= 0. \end{aligned} \tag{2.3}$$

The physical quantities of (2.3) are as follows; $\vec{v}$ is the velocity, P is the pressure, ρ is the density, ν is the kinematic viscosity, and $\vec{f}$ is an external force. To distinguish between laminar and turbulent flows, the Reynolds number Re is often analysed. It is a dimensionless quantity which estimates the ratio between inertial forces and viscous forces. It also serves as a characterisation tool for flow patterns, determining what flows are laminar and what are turbulent. As a rule of thumb, one considers laminar flows to be flows where $\mathrm{Re} < 2400$ while turbulent flows have $\mathrm{Re} > 4000$. It can be calculated from

$$\mathrm{Re} = \frac{Lu}{\nu}, \tag{2.4}$$

where L is the characteristic length, u is the relative speed of the fluid, and ν is like before the kinematic viscosity. In the zero-viscosity limit (equivalent to $\mathrm{Re} \to \infty$), the Navier-Stokes equations (2.3) are invariant under the transformation $\mathcal{L} \to \lambda \mathcal{L}$ when

$$\vec{v} \to \lambda^h \vec{v}, \qquad \nu \to \lambda^{1+h} \nu, \qquad t \to \lambda^{1-h} t. \tag{2.5}$$

Here, t is the time, λ is an arbitrary scale factor, and h is an arbitrary similarity exponent.

The key argument of Frisch and Parisi (1985) is now that since h is arbitrary, the equations allow for different values of h, and more specifically mixtures of different h. The velocity field $\vec{v}(\vec{x})$ is said to have a singularity of order $h > 0$ at the point $\vec{x}$ if

$$\lim_{\vec{x}\to\vec{y}} \frac{|\vec{v}(\vec{x}) - \vec{v}(\vec{y})|}{|\vec{x} - \vec{y}|^h} \neq 0. \tag{2.6}$$

If one lets $S(h)$ denote the set of points in the velocity field which has a singularity of order h, then $S(h)$ is the region where where the velocity is not a Hölder function of order h (Evans (2010)). Simply put, this puts only a very weak restriction on how fast the velocity field may vary between two point $\vec{x}$ and $\vec{y}$, which one would suspect from the chaotic nature of turbulence. It is common to change the notation when analyzing multifractals and let $h \to \alpha$, although they still describe the different singularities of the field/set. The hierarchy of different fractal exponents are usually analyzed using the $f(\alpha)$-curve, first suggested by Halsey et al. (1986). The $f(\alpha)$ curve is often called the multifractal spectrum, and can be though of as a function that weights the contribution from the different values of α to the total system.

As going into details about the mathematical formalism of multifractals are rather tedious and not relevant for applying the concept to a model, this will be all that is said about the formalism of multifractals. The following sections is an introduction to multifractals and fully developed turbulence from a more phenomenological perspective, with examples relevant for the work presented later. It is inspired by Schertzer et al. (2008), where one can also find a more rigorous approach than what is presented in the following.

2.2 Cascade models for fully developed turbulence

Fully developed turbulence was already before Parisi coined the term in 1985 believed to be statistically described by a multifractal hierarchy, and goes back to the notion of *big whirls have little whirls that feed on their velocity, and little whirls have lesser whirls and so on to viscosity* (Richardson (1922)). These whirls are today more commonly referred to as eddies. The term multifractal was not invented, but work had been done on the topic nevertheless, in particular by Kolmogorov in the so-called K41-theory (Tikhomirov (1991a) and Tikhomirov (1991b)).

K41-theory assumes that the energy transfer rate in turbulence is uniform in space and independent of length scale. Additionally, it is assumed that this energy transfer rate per unit mass, ϵ, has a finite non-zero value. As a consequence, Kolmogorov proposes the hypothesis that the distributions for local isotropic turbulence are uniquely determined by the average rate of energy transfer ϵ and the kinematic viscosity ν. One uses the relation that

$$u^2 \sim E_t, \tag{2.7}$$

where u is the characteristic velocity and E_t is the turbulent kinetic energy. Assuming that this is true for all scales of the eddies and dropping the t subscript for turbulent kinetic energy, one has that

$$u_l^2 \sim E_{L_l}, \tag{2.8}$$

where the subscript L_l indicates the length scale of the system at level l (the l will later be connected to the cascade level of the hierarchy of turbulent eddies). Additionally, one estimates the turnover time t_l which according to Frisch and Kolmogorov (1995) is the time at which an

eddy undergoes a significant distortion. Mathematically, one estimates it by the time it takes to move across the length scale when going at the characteristic velocity of that scale

$$t_l \sim \frac{L_l}{u_l}. \tag{2.9}$$

Once one has an estimate for E_{L_l} and t_l, one may also estimate the average rate of dissipation

$$\epsilon \sim \frac{E_{L_l}}{t_l} \sim \frac{u_l^3}{L_l}. \tag{2.10}$$

It is from this possible to derive the Kolmogorov length scale η to be (see Tikhomirov (1991a))

$$\eta = \left(\frac{\nu^3}{\epsilon}\right)^{1/4}, \tag{2.11}$$

which is the shortest scale at which turbulence occurs.

Combining this with the notion of small eddies feeding off of larger ones, one can construct a hierarchy of eddies, down to the Kolmogorov length scale η, at which scale the dissipation transforms the energy into thermal energy due to viscosity. Several models for doing this have been proposed, starting with Yaglom (1966) who did pioneering work on phenomenological models of turbulence, where the key assumption is that successive steps independently define the fraction of the flux of energy distributed over smaller scales. As a consequence, smaller eddies do not add energy, but rather adjust the energy passed down from larger scales.

To generate this hierarchy of eddies, the classical way is to start with a $\mathcal{D}$-dimensional cube $C_0^{0_\mathcal{D}}$ (generally denoted $C_l^{i_j}$), which iteratively is divided into smaller cubes. In this notation, the subscript denotes the cascade level (recursion level, denoted by l like in the previous derivation), while the superscript indicates the coordinates (here in base λ) defining the particular cube in question. An illustration can be seen in Figure 2.3. This will in general require $\mathcal{D}$ coordinates in base λ in $\mathcal{D}$-dimensional space, hence the subscript on the superscript. Keep in mind that the ratio of scales for each cascade level is determined by λ. The cube $C_0^{0_\mathcal{D}}$ is of size L_0, and the divisions occur for each step for $l = 0, 1, 2, ..., n$ into sub-cubes $C_l^{i_j}$ with $i_j = 0, 1, 2, ..., \lambda^l - 1$ and $j = 1, 2, ..., \mathcal{D}$. These sub-cubes then form a disjoint cover of $C_0^{0_\mathcal{D}}$ and have size L_0/λ^l. Letting ϵ_l denote the density of the energy flux at step l, one notes that ϵ_l should be homogeneous on each sub-eddy. In other words, ϵ_l is a step function for each step l. This distribution of energy to the next steps follows

$$\epsilon_l = \mu_l \epsilon_{l-1}, \tag{2.12}$$

where μ_l is the multiplicative increment taken for each step, and ϵ_{l-1} is the energy density at the previous step. The multiplicative increment μ_l is analogous to the additive increment δ, and it is the difference in choices of μ_l that separates the different models proposed for the hierarchy of eddies.

2.2.1 Unifractal β-model

The simplest cascade model is the β-model, first proposed by Frisch et al. (1978). This model describes eddies in real space, and most of the process is similar to what was described in

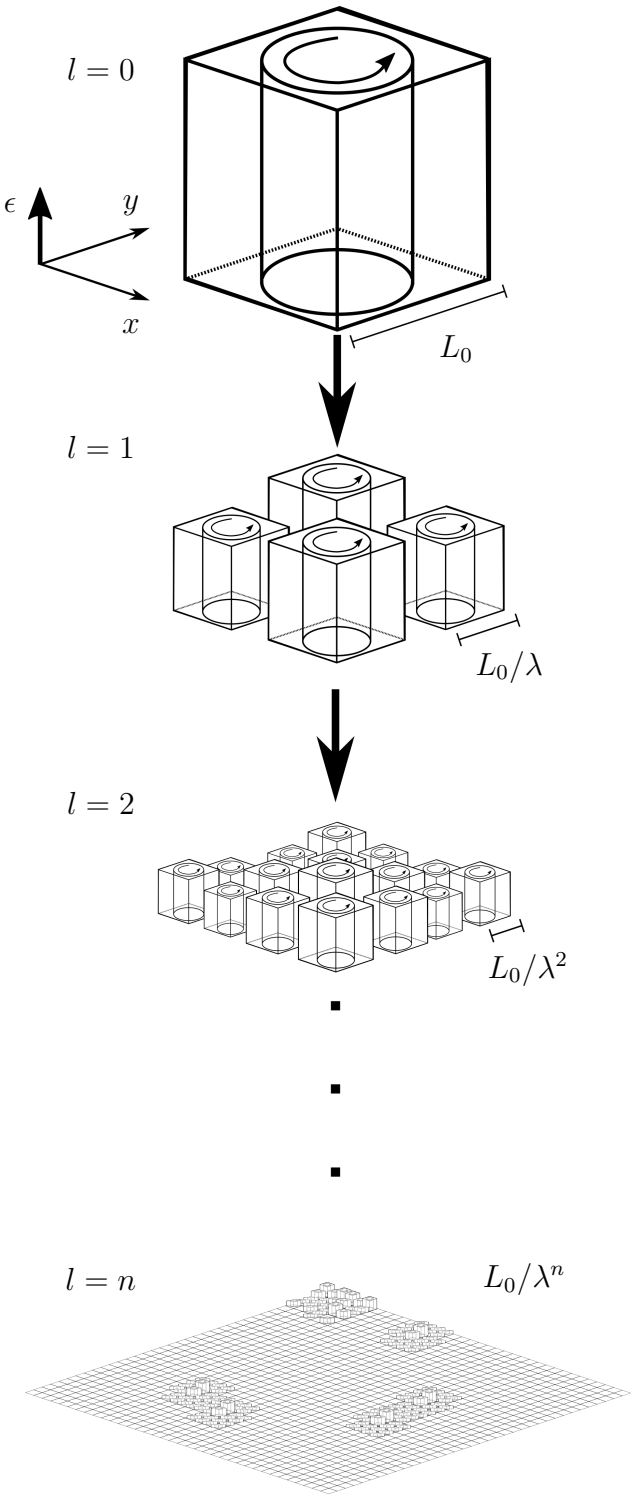

Figure 2.3: Schematic of how a $\mathcal{D}$-dimensional cube $C_0^{0_\mathcal{D}}$ representing eddies may be recursively split into sub-cubes of length L_0/λ. In this illustration, $\lambda = 2$. The kinetic energy transferred to the sub-eddies in the sub-cubes will be determined by μ_l, which is the multiplicative increment. Note that the smaller eddies cannot add energy, they only modulate the energy passed down the scales.

section 2.2. What is special about the β-model is that at each step in the recursive division, only a fraction of the volume of the mother eddy is covered by the daughters. This fraction is determined by $0 < \beta < 1$. For a fixed value of β, this builds up a set similar to the Cantor set described in section 2.1 as the number of steps $n \to \infty$. In practice, the β-model can be thought of as the daughter eddies being either dead or alive for each step, with β deciding the fraction of each. This means that after l steps, only a fraction β^l of the original fluid is still considered active.

2.2.2 Multifractal p-model

The perhaps simplest multifractal cascade model is the random β-model, where one considers β to be a random variable. This will ensure that the behavior will deviate from the deterministic Cantor set-like behavior in the original β-model. However, more sophisticated models have been proposed, and the one used in the work presented later is the so-called p-model, which was proposed by Meneveau and Sreenivasan (1987). In this model, the mother eddy of size r breaks down into $2^{\mathcal{D}}$ eddies of equal size $r/2$ (note that this is similar to setting $\lambda = 2$ is section 2.2). As before, $\mathcal{D}$ is the dimensionality of the eddy.

What separates this model from others (especially the β-model) is that the energy is now split unequally between the daughter eddies. A fraction p_1 is distributed equally among one half of the $2^{\mathcal{D}}$ new eddies, and a fraction $p_2 = 1 - p_1$ among the remaining half. It was found in the original paper that $p_1 = 0.7$. This process is then repeated until one of the daughter eddies reaches a length scale of order the Kolmogorov scale η. By this construct, there is in general a hierarchy of singularity exponents which describes the eddies, and thus the turbulent flow. This hierarchy can in general be infinite, however doing numerical simulations naturally limits it to an upper bound. This is also justified by the Kolmogorov scale η putting a lower bound for the scales at which turbulence occurs.

2.2.3 Motion of particles

Since the main interest is the dynamics of the aerosols, one has to investigate the effect of the velocity field on the movement of the particles. There are in general two contributions to the motion, namely advection and diffusion. Advection due to the influence of the velocity field, and diffusion due to the size of the aerosols and the kinetic energy of the molecules in the air.

Advection

When particles are submerged into an air flow, they are subjected to drag forces from that flow. These forces may be calculated using the drag equation

$$F_d = \frac{1}{2}\rho_{\text{air}}(v_{\text{rel}})^2 C_d A. \tag{2.13}$$

Here, ρ_{air} is the mass density of air, v_{rel} is the velocity of the air flow relative to the velocity of the particle, C_d is the drag coefficient (specific for the shape of the particle), and A is the projected area of the particle along the direction of the flow. The force F_d will as a result also act in the direction of the flow.

The forces acting on a particle in a fluid will cause the particle to have a terminal settling velocity, which from Seinfeld (1986) is on the form

$$v_t = \frac{1}{18}\frac{d_p^2 \rho_p g C_c}{\mu}, \tag{2.14}$$

where d_p is the diameter of the particle, ρ_p is the density of the particle, g is the gravitational acceleration, μ is the dynamic viscosity, and C_c is the Cunningham correction factor. The Cunningham correction factor is determined by $C_c = 1 + \frac{2\lambda_{\text{mfp}}}{d_p}[1.257 + 0.4\exp(-1.1 d_p/2\lambda_{\text{mfp}})]$, where λ_{mfp} is the mean free path of molecules in air. It is in general a number going to 1 as d_p increases. For particle with a diameter of 2 μm, C_c is approximately $\mathcal{O}(1)$. It has therefore for simplicity been set to 1 in the simulations performed in this thesis.

Diffusion in air

From Seinfeld (1986), one has that for particles diffusing in air follows the diffusion relation

$$D = \frac{kTC_c}{6\pi\mu r_p}, \tag{2.15}$$

where k is the Boltzmann constant, T is the absolute temperature, C_c is the Cunningham correction factor, μ is the dynamic viscosity (of air) and r_p is the particle radius. For the lighter BC particles, C_c is of $\mathcal{O}(10)$, so it was set to 10 when calculating the diffusivity for the BC particles/clusters.

2.3 Diffusion-limited aggregation

As described in Section 1, one of the main goals of this work is to understand the mixing of BC clusters and mineral dust particles. In order to generate the BC clusters which are later used in the mixing, an algorithm for diffusion-limited cluster aggregation (DLCA) describes the irreversible growth process determined by random walkers forming a cluster.

Diffusion-limited cluster aggregation is an algorithm based on the diffusion-limited aggregation algorithm (DLA) proposed by Witten and Sander (1981). DLA is an algorithm describing irreversible growth process where the factor limiting the growth is the amount of mass available in the system. It is an algorithm based on the Eden model proposed by Eden (1961), but now the aggregation is determined by random walkers. The DLA algorithm is as follows: A stationary seed particle is placed in the middle of a domain. This particle will be the basis for the growth of the cluster. Another particle is launched at some distance from the seed particle, and this launched particle will perform a random walk. This distance can in principle be infinitely far from the seed particle, but it is for practical reasons usually set to be relatively close to the seed particle/cluster. The walking particle will continue the walk until it hits the seed particle, at which point it becomes a part of the cluster. This process of launching random walkers are repeated until the size of the cluster is satisfactory. Usually, one will restart the random walker if it wanders too far from the seed particle, in order to speed things up.

The modification of DLA to DLCA is that the one no longer looks at an initial, stationary seed particle, but rather an initial distribution of particles. Instead of launching successive random walkers from a distance, one rather lets all the particles in the distribution perform random walks. Without any additional effects the particles may diffuse as random walkers, with

step lengths determined by (2.15). To incorporate the effects of the turbulence, the contribution from the velocity field is accounted for, giving a modification to step length and step direction.

When simulating this numerically, one uses the result shown by Einstein (1905), that random walks and diffusive processes are connected. If the steps Δx taken by the random walker are sufficiently small, then random walks and Brownian motion are related through

$$D = \frac{(\Delta x)^2}{2\Delta t}, \tag{2.16}$$

where D is the diffusion constant (also called diffusivity), Δx is the step taken by the walker, and Δt is the time it takes the walker to perform one step. Equation 2.16 explains how the random walkers proposed by Witten and Sander (1981) in their diffusion limited aggregation (DLA) model can be part of a diffusion process. The cluster formed by this process displays the fractal structure as described in Section 2.1.

When looking at (2.16), it should be pointed out that one could possibly have avoided modeling the turbulence as a multifractal velocity field (as described in Section 2.2). By letting the step lengths Δx follow a Lévy flight (Lévy and Borel (1954)), and adjusting the distribution for the directions, one could possibly model the turbulence in a more computationally efficient way. A Lévy flight is the situation where Δx has a probability distribution with a heavy tail (also called a fat tail). The problem would be that one would have to incorporate correct correlations in the distributions, which is highly non-trivial. Although some work has been done taking this approach of using a Lévy flight to model turbulence/diffusion processes (Shlesinger et al. (1987)), it was assumed that using the superimposed multifractal velocity field was more straight-forward and conceptually simpler than the Lévy flight approach.

Chapter 3

Method

In this chapter the method for simulating the coagulation rate of the BC clusters and mineral dust particles is presented and discussed. This means both the physical assumptions made for the problem, as well as the technical solutions like the choices of algorithms and methods for simulating this on a computer. To begin with, the general assumptions are stated, and arguments are made for why these assumptions are necessary. Then the choices made about collision detection algorithm and the method for simulating turbulence is presented.

3.1 General assumptions

To limit the complexity and the technical challenges of the simulations, all the simulations are done in two dimensions. This will also reduce the simulation time required, and is done since this is a first attempt to simulate the proposed physical system, and one would like to have results within a reasonable time frame. It should be pointed out that the simulated dimensions are in a horizontal xy-plane, with the z-axis pointing upwards. This is shown in Figure 3.1, where also the fact that there must be several layers to resemble a three-dimensional system is displayed. Included in this assumption is thus that all gravitational effects are neglected in the mixing dynamics, except for the settling/deposition of mineral dust particles. As dust particles fall out of the plane, others are introduced at random positions to simulate particles falling from layers above that of the simulation. For simplicity it is assumed that the dust particles falling into the layer will not have any BC clusters attached to them, meaning they come pure into the mixing plane. All particles are assumed to be spherical. The mineral dust particles are assumed to move in and out of the plane instantaneously, similar to if they were cylinders falling through a plane (constant radius), although they will fall out after some time τ_{fallout} determined by the amount of time it would take the particle to fall a distance equal to its diameter according to the settling velocity v_t (2.14). All clusters are assumed to be rigid, and it is assumed that there will be no rotations (momentum transfer from collisions). When collisions occur, it is assumed that the colliding particles/clusters will always stick to each other and form a new cluster. Finally, there will be no folding of the clusters formed, as the folding process is very complex to simulate properly.

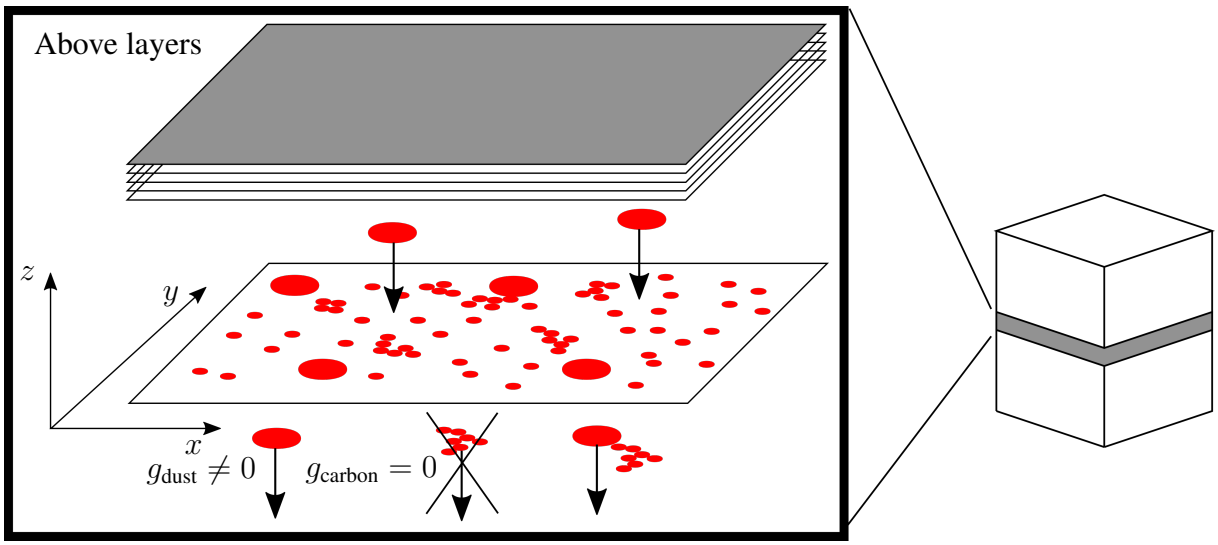

Figure 3.1: Schematic of the simulated situation, where the particles are mixing and moving along in the xy-plane, although they are still part of the volume represented by the cube on the right. The heavier dust particles are eventually affected by gravity so that they fall out of the plane, and are effectively deposited. This is not the case for the BC particles, which remain in the plane until they can be transported out by a mineral dust particle. The particles falling out are modeled to be redistributed by particles falling into the plane at random positions. For the full three dimensional system, one has a multitude of layers in which the simulated mixing and deposition occur. Note that it is assumed that there are no clusters falling into the plane, only single particles.

3.1.1 System assumptions

Another assumption to make is whether or not to use periodic boundary conditions (PBC) on a closed system. The strengths of a bounded system of PBC are that one has complete control over where the particles are, and the turbulence which affect them is easier to simulate. There is also no upper bound on the physical time one can simulate, as PBC ensure everything is stable. Alternatively, one can have an open system (open domain, OD) where one simulates a source of BC particles emitted into the atmosphere, and they undergo diffusion and advection on an OD. The advantage of this is that it is intuitively closer to the physical system one tries to simulate, however it sets other requirements for the collision detection algorithm. To put it in other terms, a grid-based algorithm is no longer viable, and the work done in the project thesis (Berntsen (2015b)) has to be improved to accommodate this situation. Instead, an algorithm using a quadtree structure has been used, which is presented in detail in section 3.2.1.

An additional consequence of running open system simulations are that there will be a density gradient in the system which would not be there for the closed system with PBC. The distribution of mass in an open system is shown in Figure 3.2. This reduces the generality of the results, and restricts the simulations to the regions around the source of the BC clusters. It also forces an upper bound on the physical time one can simulate, as increasing this must correspond to an increase in system size. If one wants to use mass concentrations consistent with what is reported by experiments, while one ensures that the domain is populated by dust particles, this will quickly scale out of hand. To look at both cases, and to avoid having to make unnecessary assumptions, both cases were implemented to be able to compare their results.

From Scarnato et al. (2015) and Ryder et al. (2013), one has a good estimation of the size of

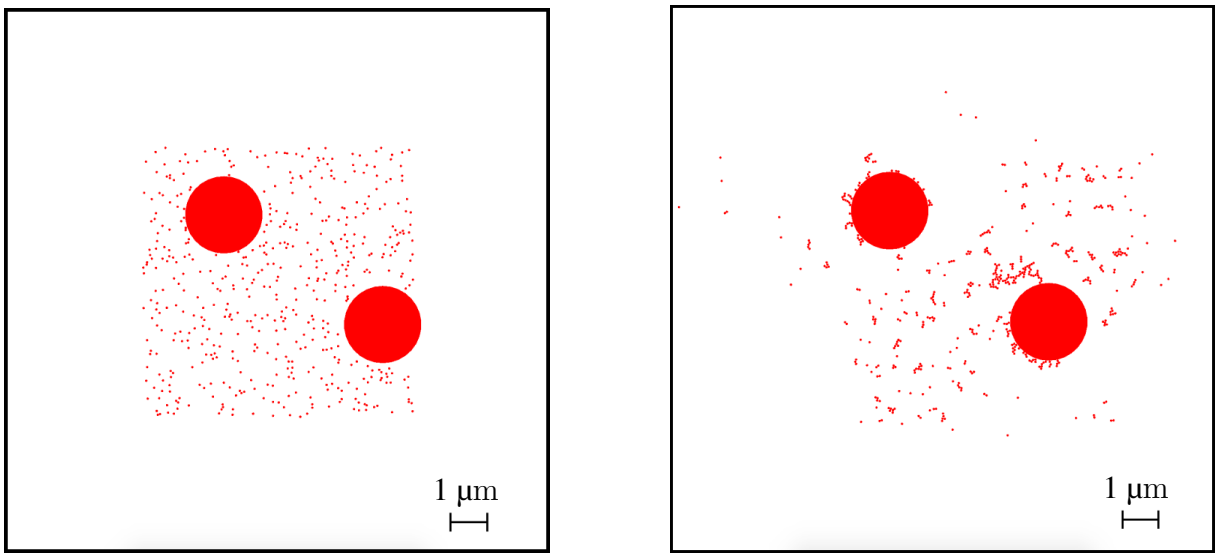

(a) Initial distribution of the system at $t = 0$.

(b) After $t = 1.445 \times 10^{-5}$ seconds.

Figure 3.2: Illustration of how the system was simulated. Both the open system and the periodic boundary simulations started with the BC particles highly concentrated far from the boundary. For the open system simulations, the distance from the boundary of the domain initially distributed by the carbon particles were set to be so large that the particles would never reach the boundary during the physical time simulated. This is not necessary for the periodic boundary conditions simulations. In this illustration, the carbon particles are scaled up to $r_{\text{carbon}} = 30$ nm to increase the visibility on the figure as it is only included for illustration purposes. The total domain is in this case 1400 units with 1 unit being 10 nm, and the particles are distributed in the middle fourth of the domain ($x \in [\frac{x_{\text{size}}}{4}, \frac{3x_{\text{size}}}{4}]$, $y \in [\frac{y_{\text{size}}}{4}, \frac{3y_{\text{size}}}{4}]$). There are $N_{\text{dust}} = 2$ dust particles, and $N_{\text{carbon}} = 500$ carbon particles.

BC monomers, what cluster sizes are observed experimentally, as well as what sizes of mineral dust particles one might expect. Once one knows the approximate size of the particles involved in the simulation, it is possible to calculate the diffusivity of the particles in air at standard temperature and pressure from equation (2.15). As there are several uncertainties involved with the sizes of the particles, the Cunningham correction factor is for simplicity set to unity for the larger dust particles, while it was set to 10 for the BC. From equation (2.16), it is evident that one may calculate the step length of the particles diffusing by determining a time step Δt. Thus the time steps of the simulations have been chosen so that the step length Δx is as large as possible to increase the speed of the simulations, however still maintaining a reasonable resolution for the dust particle lifetimes τ_{fallout}. It is assumed that it is sufficient that $\Delta t < 0.1\tau_{\text{fallout}}$ to maintain this resolution. The diffusion coefficients appear to be in good agreement with those presented in Seinfeld (1986), indicating that at least the order of magnitude is correct in the simulations.

3.1.2 Assumptions about aerosol sizes and concentrations

Although it may be of interest to try to find a general relation between the deposition rate of BC and the dust concentration of the system, the problem stated in Section 1 is rather specific. To try and give the best possible answer to it, it seems evident that the more specific one can be, the better. As a consequence, the concentrations of both BC and mineral dust needs to be in accordance with what has been experimentally observed. Although many of the studies done on the topic have not necessarily been done in the exact locations one is interested in, they still give a good estimate of what values one might expect.

It is worth noting that there have been some difficulties when trying to find the sizes of the mineral dust aerosols, as the main interest of previous research appears to have been on the optical properties of the mineral dust. Some of the studies (Maring et al. (2003), Sokolik and Toon (1996), Li et al. (1996), Clarke et al. (2004)) reports the optical properties of mineral dust, and how it is dominant in radiative forcing in the atmosphere. In for instance Maring et al. (2003), the size distribution is reported, however only up to $d_{\text{dust}} \approx 10\ \mu\text{m}$. This is due to the optical properties of particles of aerodynamic radius up to 10 μm, which are commonly called PM_{10} particulates. For particles exceeding this size, the optical properties is of less interest, as the particles does not scatter the incoming light in the atmosphere to the same extent. Additionally, health hazards of inhaling such particles (Schwartz and Neas (2000)) are less than the PM_{10} particles, which means that there has not been much incentive to study larger particles. There is still reason to believe that locally, mineral dust aerosol sizes may exceed this. It has been observed by Ryder et al. (2013) for a study done over western Sahara. There was found airborne Saharan dust which extends size distributions to 300 μm, which suggests that there are heavy dust particles eligible for deposition of BC clusters.

To begin with, it was assumed that the BC particles would have a radius of the order 10 nm, so r_{carbon} was initially set to this value. Since the number concentration C_{dust} of mineral dust particles would be dependent on the size of the particles, and one would (as discussed later) be interested in having a high number concentration, the radius $r_{\text{dust}} = 1\ \mu\text{m}$ was used. This reduces the settling velocity of the particles, and may in that regard effect the rate of deposition, but is done in order to obtain results that can suffice as a first estimate.

Although the mineral dust particles are in reality not identical, it was assumed that they were. The size distributions reported show that the sizes usually follow a log-normal distribution, however it was for simplicity assumed that the reported mass concentrations were from equally sized particles. This will skew the number concentrations somewhat, but like when determining

the mineral dust radius, this is done to get an initial estimate.

Dust concentrations

Concerning the concentration of the mineral dust, it is assumed that using the reported concentrations from experimental observations will give the closest replication of the physical system for the simulations. There have been quite a lot of studies reporting on the matter, for instance (Tegen and Fung (1994), Marticorena et al. (2010), and Alpert and Ganor (2001)). Since these are experimental measurements, the numbers are reported in μg/m^3 which have to be mapped to the two-dimensional equivalent in order to correspond with the simulations. To do this, one multiplies the particle concentration by a typical length, in this case the diameter of the dust particles d_{dust}. The study by Marticorena et al. (2010) investigates the mineral dust concentration over Senegal, Niger and Mali, and reports that the median concentrations were between 75.3 μg/m^3 and 87.2 μg/m^3, whereas the overall measured peak was 4020 μg/m^3 in Niger. The other peak measurements were around ≈ 2000 μg/m^3. It should be noted that these regions are located in the Southwestern part of the Sahara, and can be considered to be in the vicinity of the Saharan desert. The peak measurements are in accordance with the results found by Alpert and Ganor (2001), a study conducted in Eastern Sahara and the Middle East region. Although it does not from a physical perspective seem reasonable to base the simulations on the peak concentrations, the simulations were to begin with based on these peak values in order to obtain results in a reasonable amount of time.

To calculate the number of dust particles required in the simulations, initially a concentration of $c_{\text{dust}} = 2000$ μg/m^3 was used. This value was used mostly to have simulations with known physical quantities were the chance of having significant results are maximized. In a study done by Menut et al. (2007), the cumulative mass concentrations were reported for sites in Niger and Capo Verde. In addition to having measured high concentrations in during the peaks, one may assume that all particles of radius $r_{\text{dust}} > 1$ μm (not only up to 10 μm) could potentially be possible transporters for the BC clusters. The results from Menut et al. (2007) suggest that the cumulative mass of mineral dust may be so high that one could make an argument for using a number as high as $c_{\text{dust}} = 4000$ μg/m^3 to maximize the possibility of collisions. It was therefore deemed that one could possibly base the simulations on this higher number, but to start out with the lower concentrations.

To be able to calculate the number of mineral dust particles corresponding to this concentration, one must make an assumption about the mineral dust mass density. In the work done by Hansell Jr. et al. (2011), the mass densities of the most common constituents of mineral dust are listed. Since there may be various fractions of the different constituents, the mean density (excluding Hematite since it deviates from all the others) is taken as an estimate for the dust particles used in the simulations. As a result, $\rho_{\text{dust}} = 2.67$ kg/m^3. Other studies such as Tegen and Fung (1994) reports the density to be $\rho_{\text{dust}} = 2.5$ kg/m^3. Once again, since one is interested in maximizing the possibility of collisions, one uses a value for ρ_{dust} at the lower end of the spectrum, as this will maximize the number of particles in the system. There is not really a physical argument to do this, other than since one needs to use a density, it may very well be a reported value which increases the chances of collisions. Using a dust density of $\rho_{\text{dust}} = 2.5$ kg/m^3, this yields a number concentration of $C_{\text{dust}} = 360$ particles/m^2 for $c_{\text{dust}} = 2000$, and $C_{\text{dust}} = 764$ particles/m^2 for $c_{\text{dust}} = 4000$. These numbers seem more accurate than they really are, partly because the approximation of identical particles and partly because the measurements to begin with would have some degree of uncertainty.

Using the commonly reported results on mean concentrations, the number concentration of dust particles should be ≈ 10 particles/m^2. If one on rather use the peak measurements as found by Ryder et al. (2013), the number should be ≈ 500 particles/m^2. It is therefore stressed that the values used in simulations are the peak values for practical reasons, as a compromise between the reported values and the wish to answer the problem of Section 1. Finally, one should stress that as reported by Gillette et al. (1974), there is a relation between the wind speed and dust particles in the atmosphere. This has not been taken rigorously into account, but it is kept in mind when determining the turbulent mixing which is thought to be dependent on the wind speed.

Carbon concentrations

Similarly, one should have an estimate for the concentration of BC. For the BC particles, the mass density ρ_{carbon} of amorphous carbon is used, as listed by Lide (2004) and Bond et al. (2013) to be between 1.5 and 2 kg/m^3. For the BC concentration, different approaches were taken for the open system simulations and the periodic boundary condition simulations. For the former, it is assumed that the BC particles have a very high local concentration, resembling a source for BC particles. This is strictly speaking not the case for the PBC simulations, where the BC particles are assumed to be evenly distributed. From experimental results, it is shown that there is usually only clustered BC which is found attached to dust particles, meaning that in order to replicate the results found by experiments, one must have a mechanism for clustering the particles. To try to accomplish this, a high concentration of BC is distributed to begin with in both cases. This is in agreement with modeling a source, but will mean that the carbon concentration will be artificially high to begin with for the PBC simulations. The results for short times should therefore be treated with caution.

As was the case with dust particles, one would still like to know the particle concentrations which exist in the actual physical system. In order to estimate this, an analysis was done using numbers from Algeria, as reported in Elvidge et al. (2016). Here, the annual amount of burned natural gas is stated to be 6.0×10^9 m^3, along with the number of flares in total which is $N_{\text{flares}} = 150$. Combined with an emission rate of black carbon of 2.3 g/m^3 burned natural gas from Huang et al. (2015), one may estimate the emitted amount of BC particles per second at each flare. For this estimate, a density of $\rho_{\text{carbon}} = 1.5$g/cm^3 was used for BC particles with $r_{\text{carbon}} = 10$ nm. If one assumes that wind comes in to the plume at 5 m/s along the x-axis, a rapid turbulent mixing in the y-direction ($D_y = 0.1$ m^2/s), and the heat released increasing the expansion along the vertical z-axis to $D_z = 20$ m^2/s, one can estimate the number of BC particles per m^3. By once again looking at a plane of height d_{carbon}, one finds the number of particles per m^2 as shown in Figure 3.3. Although this is a very rough estimate of the number of BC particles one might expect within the plume from a gas flare, with very generous expansion of the volume from the diffusion coefficients, it is a too large number to realistically model. The concentration does drop off rather rapidly, and modeling the plume and the source as it emits the BC properly is outside the scope of this thesis. As the main climatological effect one wishes to investigate is the change of albedo once the BC is deposited, it seems most reasonable to simulate scenarios where the BC is diluted and transported. This is because once the BC are transported, it will potentially be deposited on a larger area, meaning the effect is potentially greater.

There is still a problem of initial concentration of BC, as the only conclusion one can draw from Figure 3.3 is that there is an abundance of BC, and the concentrations seems to be way

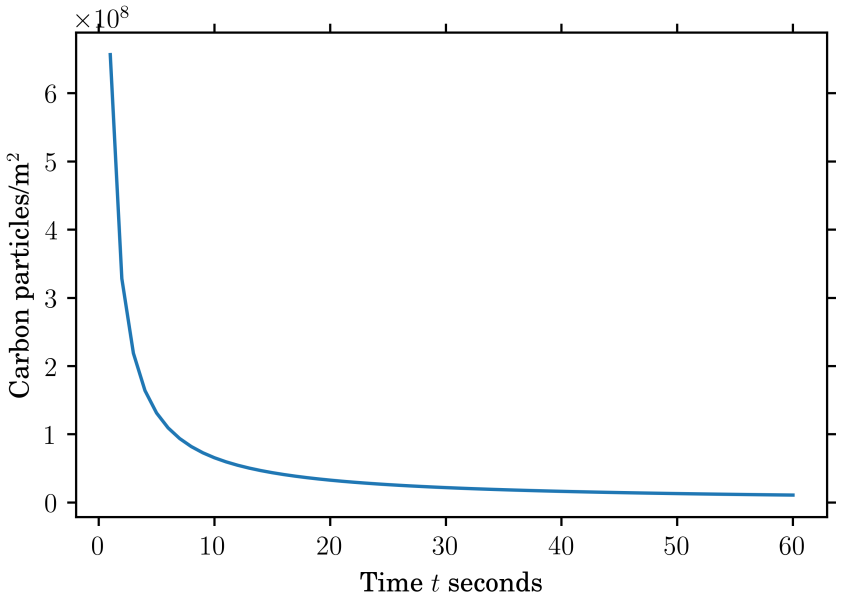

Figure 3.3: Rough estimate of the concentration C_{carbon} of BC particles within the plume from a gas flare as a function of time t. It seems apparent that there is an abundance of BC particles so that modeling the entire amount would be impractical.

too high for modeling in this thesis. One may set the concentration as high as one would like, depending on the distance from the source. Due to this, and the fact that modeling the estimated concentrations is not possible, there is a certain freedom when setting the BC concentration, but it should be in a range so that the simulations run reasonably fast in order to obtain some actual results.

3.1.3 Assumptions about turbulence

For the turbulence modeled in this thesis, it is assumed that superimposing a dynamic, multi-fractal velocity field is sufficient to reassemble the turbulence found in the real system (see 3.3.3 for more on the implications of this). It is to begin with assumed that the velocity of the winds in the system are rather low, meaning that one has weak turbulence. The velocity u_0 is not the actual wind speed, but represents the energy driving the turbulent mixing, contributing to the turbulent kinetic energy. Wind speed is thought to be related to the amount of mineral dust particles, especially in the case of heavier particles, since wind transport is the main transport mechanism for the mineral dust from the soil to the atmosphere. Although it is assumed no vertical effect on the mixing, it must be assumed that wind speed is in some way related to the amount of mineral dust particles, at least locally. This imposes a problem for the open system simulations, where a source is assumed to be stationary in space. An approach where one only looks at the relative motion is in that case not possible.

In some of the studies reported in the previous section, the measurements are made far from the origin of the mineral dust aerosols. From this, it is assumed that a low velocity u_0 may be reasonable for the periodic boundary conditions simulations. When simulating the source, the wind speed is much harder to make assumptions about. It has not been the scope of this work to look at the exact relation between wind velocity and particle concentration, so the assumptions

made about this relation are rather weak, but ultimately based on previous studies (Gillette et al. (1974)).

It should also be noted that turbulence in general is not well understood, and especially two-dimensional turbulence dynamics. This is extensively discussed in Bohr et al. (1998), and will not be discussed more in this section. It is brought up to argue that there will always be uncertainties in the results, due to the lack of understanding of turbulence.

3.2 Collision detection algorithm

In addition to decide on what the system one would like to simulate is, a technical implementation of the simulation has to be performed. The method used for checking collision between BC particles, clusters and mineral dust particles are based on chapter 7.3 in Ericson (2004). The most common approach to the problem of collision detection is to do a two phase detection, split into the broad phase and the narrow phase. In the broad phase, one does a coarse filtering of the domain, detecting what particles may possibly collide. The particles eligible for collisions are then investigated further in the narrow phase, where an exact collision detection calculation is performed. The broad phase collision detection algorithm used in this thesis is a quadtree (see section 3.2.1).

3.2.1 Broad phase collision detection

To be able to detect a collision between two particles, one has to calculate the distance between the two. If they are particles with extent and not only points, one has to allow for the radii of the particles to be included in the distance, meaning the minimum distance between them (and thus the criteria for a collision) is $d_{1,2} = r_1 + r_2$ where r_1 and r_2 are the radii of the respective particles. If there are more than two particles, one will have to check every distance between every particle. As a result it will have a computational complexity of $\mathcal{O}(n^2)$.

The main motivation for having a broad phase collision detection is to reduce the number of checks needed for each particle under investigation. By doing a computationally cheap, rough filtering of which particles are eligible for collision, one reduces the computational complexity significantly.

There are several ways to perform a broad phase collision detection, but the two main methods suitable for the problem at hand are grid-based collision detection methods and quadtrees. Both methods have different advantages and disadvantages, but ultimately the method of choice must be the best suited for the specific problem. Although grid-based methods are considered to be faster (at least on modern CPUs) and better scaling with number of objects to check for collisions, it is hard to scale the physical size of the system as it will eventually require too much memory to store the grid. The choice therefore fell on the quadtree method, which is easier to scale in physical size, but an older and slower algorithm for the actual collision detection and scales worse than the grid-based method with respect to number of objects.

Quadtrees

The quadtree-algorithm is a way of spatially partitioning a domain. This is done to limit the number of exact collision calculations required for each particle, which as previously explained is in general a computationally intensive operation. The motivation behind the spatial partitioning is thus to try and select possible collision targets from a small area around the particle one is

currently investigating, which in turn will reduce the computational complexity. The quadtree is as the name suggests a tree structure where all nodes have 4 children, as the space is divided into 4 quadrants. As will be explained in the following section, there are rules for when the node must be split into 4 children.

Building a quadtree

To begin with, one has to define a domain of interest. Within that domain, one distributes particles, and the fundamental idea behind the quadtree algorithm is to keep track of where these particles are in space, and use this information to limit the number of checks required. The algorithm sets rules for how many particles can be within a quadtree domain at the same time (see *capacity* in Figure 3.4). To illustrate this, the case where the algorithm allows for one particle in a quadtree domain is shown in Figure 3.5. The rules are made so that there can be an amount up to *capacity* of particles within each domain, meaning that empty quadtree domains are allowed. In the example shown in Figure 3.5, there can be at most one particle in each quadtree domain, meaning that in this case the particles are only stored in the leaf nodes of the tree (see Figure 3.4). For practical matters, one usually sets the limitation to be greater than 1, meaning one allows for storage of particles in internal nodes. This is due to the trade-off between having to iterate over many particles per level, or having a huge number of levels. Modern CPUs are very fast at iterating, so one has to find a *capacity* that optimizes the speed in practice, and not only in theory.

However, at some point the amount of particles within a quadtree domain exceeds the set limit. Then the procedure is to split the domain into 4 new quadrants, each a new quadtree domain (hence the name *quad*tree). To put it differently, the program recursively divides the total domain (bounding the root node) into as many subdomains that are required, given the allowed number of particles per subdomain (node). Now, since one is interested in modeling cluster dynamics, and not only single particles, one has to modify this to allow for clusters. Allowing for clusters can be done in a number of different ways, the one chosen here is by the axis aligned bounding box (AABB) method, which means the area of the cluster is represented by the smallest AABB that covers the cluster. The collision detection can then be reduced to checking if two squares overlap. This is illustrated in Figure 3.6. It should be pointed out that using this representation for the areas of the clusters is possible because of the narrow phase collision check, which will correct the erroneous detections of the broad phase. One should also note that single particles are also modeled as clusters, as one can also see in Figure 3.4, where *objects* are *Clusters*.

In the special case where a particles is placed exactly at an intersection between domains, the extent of the cluster will ensure that it can be found from all of them. In other words, it is placed only in one of them, but which one will be irrelevant due to its area. The area can be found from all domains in the intersection.

Searching a quadtree

As each domain is defined by the area they span, it is relatively fast to search this tree to check for potential collision targets. This is because since each cluster is represented by an AABB, it is enough to check intersection of rectangles to check for collisions. When searching the quadtree, one defines a region of space (defined by an AABB) and does a top-down search. The search routine checks to see that the quadtree region of the tree intersects in some way with the

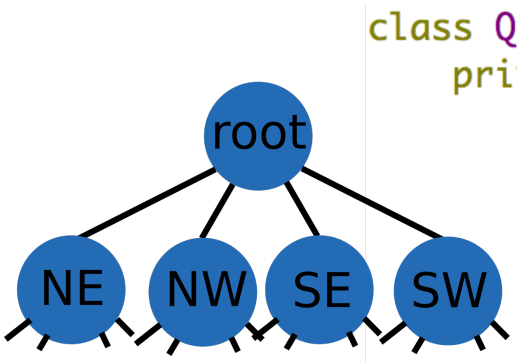


```
class Quadtree{
    private:
        Quadtree* nw;
        Quadtree* ne;
        Quadtree* sw;
        Quadtree* se;
        AABB area;
        std::vector<Cluster> objects;
        static constexpr int capacity;
```

Figure 3.4: The tree structure of the quadtree when implemented.

search region, and will then add all clusters stored within that node. It will then recursively call the search on its children nodes, drilling down the tree until it reaches the leaf nodes. By then, all clusters within the region defined by the search AABB will have been added to a list. This is the list that will later be used in the narrow phase collision check.

Periodic boundary conditions

To have the possibility to do PBC simulations, the quadtree algorithm had to be able to handle PBC. This poses a problem in the search routine, as not only would one have to take into account that the shortest distance between two clusters could be across the boundary, but also the AABBs representing the areas of the clusters in the quadtree. There are several ways to solve this problem, but the one chosen in this work was to allow each cluster to have up to 4 AABBs representing its area. These AABBs can then be placed individually in the quadtree, so that the search algorithm works as intended. Unfortunately, this also necessitates keeping track of what clusters are crossing what boundaries, in order to split or merge the AABBs. Finally, one also has to keep track of this when two clusters collide, to make sure that the resulting AABBs are correct.

3.2.2 Narrow phase collision detection

For the narrow phase collision detection, the method proposed by Kuijpers et al. (2014) for random walking particles has been used. It is illustrated in Figure 3.7. To arrive at this result, one must remember that the clusters perform a random walk at each iteration, and the fact that all clusters are made up by particles. A step direction $\alpha \in [0, 2\pi]$ (defined as seen Figure 3.7) and step length L_{free} (the step length performed if the particle can move freely) is calculated from the contributions of both diffusion and advection for each cluster at the start of every iteration. At that point, both the coordinates of the particle (x_0, y_0), and those of the potential targets (x_p, y_p) are known (from the broad phase collision detection, where all post-step AABBs are added to the quadtree after a step has been performed). Note that for this calculation, if the particle one investigates is part of a cluster already makes no difference. The distances a and b are found from geometric inspection of Figure 3.7, giving

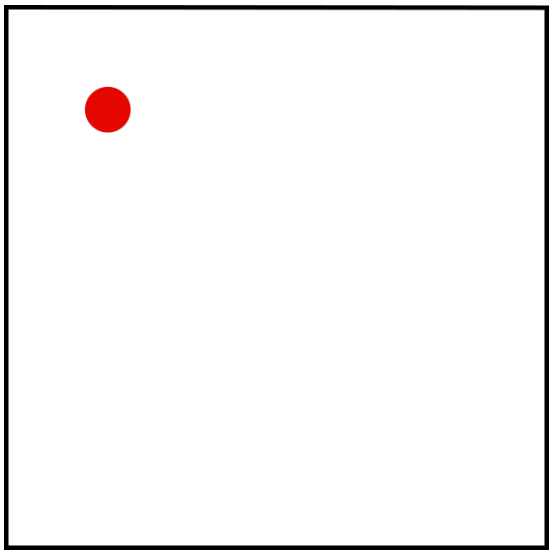

(a) To begin with, one only has a single particle in the domain. This is unproblematic, since the quadtree allows for this, and everything is according to the rules.

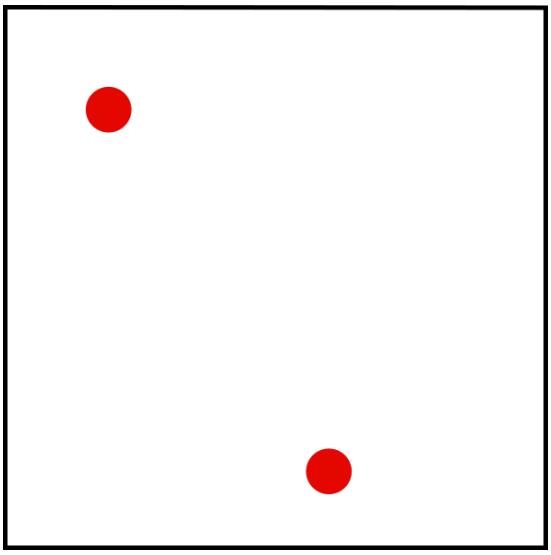

(b) When a second particle is introduced, the algorithm has a problem, since there are now more particles in the domain than what is allowed.

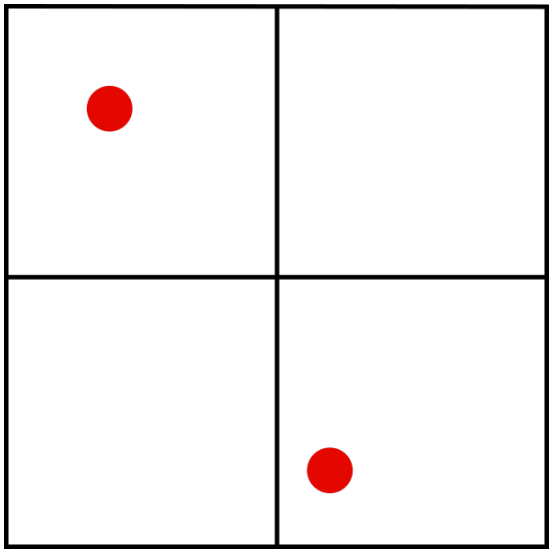

(c) To solve this, the original domain of the quadtree is split into four new domains, which ensures that the rules are maintained. Note that there is no rule against empty domains, only that the amount of particles cannot exceed a set value (1 in our example).

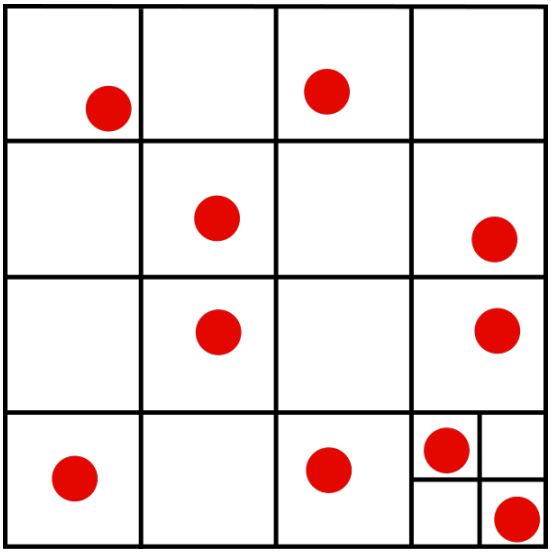

(d) As more particles are added, the domains are split again, and the process goes on.

Figure 3.5: Illustration of how the quadtree algorithm work.

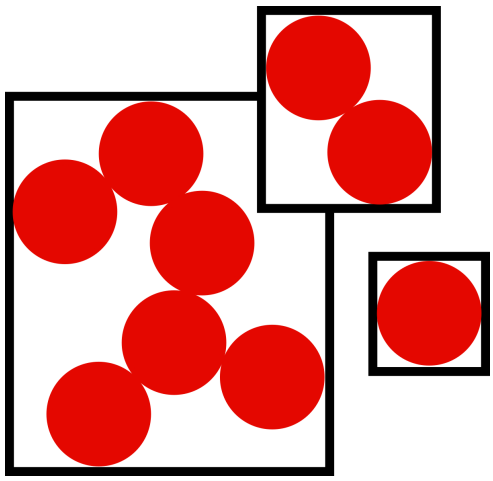

Figure 3.6: How the extent of the clusters are modeled. Note that even though the bounding boxes intersect, the clusters will not necessarily latch, as there is still some distance between the actual clusters.

$$a = x_p - (x_0 + L_{\text{hit}} \cos(\alpha)) \tag{3.1}$$
$$b = y_p - (y_0 + L_{\text{hit}} \sin(\alpha)). \tag{3.2}$$

Inserting (3.1) and (3.2) into $d_p^2 = a^2 + b^2$ and rearranging gives

$$\begin{aligned} d_p^2 =& L_{\text{hit}}^2 + 2\left[(x_0 - x_p)\cos(\alpha) + (y_0 - y_p)\sin(\alpha)\right] L_{\text{hit}} \\ &+ \left[x_0^2 + x_p^2 + y_0^2 + y_p^2 - 2(x_0 x_p + y_0 y_p)\right]. \end{aligned} \tag{3.3}$$

This can be written on the form

$$AL_{\text{hit}}^2 + BL_{\text{hit}} + C = 0, \tag{3.4}$$

with coefficients defined by

$$A = 1 \tag{3.5}$$
$$B = 2\left[(x_0 - x_p)\cos(\alpha) + (y_0 - y_p)\sin(\alpha)\right] \tag{3.6}$$
$$C = (x_p - x_0)^2 + (y_p - y_0)^2 - d_p^2. \tag{3.7}$$

As the clusters are simulated to be rigid, the step L_{hit} which causes the cluster to move the shortest is the one that will occur. As a result, one must perform the collision calculation for all particles in the cluster under investigation, before one can perform the step. If equation (3.4) only has a negative solution, or a solution $L_{\text{hit}} > L_{\text{free}}$, the function will return a step of length L_{free} which will then be performed. If not, a step of length L_{hit} is taken and a collision happens.

Once the step length is calculated, the cluster will move the appropriate length in the given direction. In the event that it will collide with another cluster, the clusters are merged. That includes updating the list of particles belonging to the cluster, the AABBs spanned by the new cluster, and conservation of momentum.

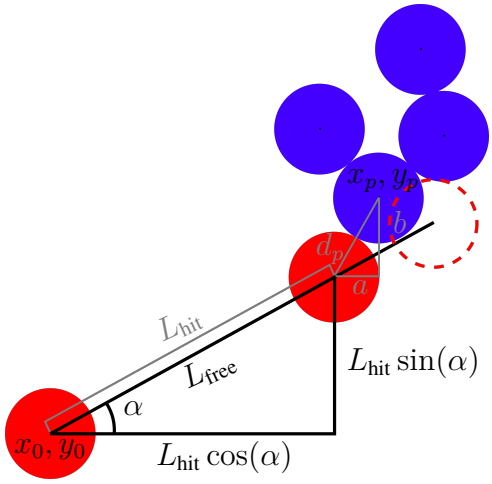

Figure 3.7: Schematic of the hit calculation. Here, the red circles are the positions of the particle one is currently investigating, and the blue are particles already in the cluster. The particle under investigation is launched from position x_0, y_0 in the α direction with the horizontal plane. The dashed red line indicates where the walking particle would end up, if it was to take a full step of length L_{free}. As the particle under investigation will collide with the particle located in x_p, y_p, it cannot do the full step, but rather a smaller of length L_{hit}. The distance $d_p = r + r_p$ is the distance between the center of the particles, while a and b are geometrical distances.

3.3 Modeling turbulence

To numerically simulate fully developed turbulence, the multifractal method described in Section 2.1.2 was used. In particular, the p-model suggested by Meneveau and Sreenivasan (1987) was used to generate a multifractal velocity field. A brief description of this method is included for illustration purposes, but for a more detailed analysis and validation of the method, see the original paper.

The method is based on the multifractal cascade way of describing the energy dissipation in fully developed turbulence, and is described in Section 2.2.2. One attempts to estimate the rate of dissipation ϵ (2.10) by investigating the flux of kinetic energy from large eddies to smaller ones, until one reaches the Kolmogorov length scale η (2.11). This approach was first introduced by Kolmogorov, in the so-called K41 theory on fully developed turbulence.

The two-dimensional p-model is illustrated in Figure 3.8, which takes into account the fact that what is modeled are not the actual eddies, but rather the turbulent kinetic energy for each eddy. The representation is thus straight arrows instead of whirling eddies. This is a simplification done in order to be able to model the velocity field resulting from the kinetic energies. The direction of the velocity is set to be random for all eddies, as an initial modeling of the isotropic turbulence.

As the two-dimensional p-model requires a splitting of the spatial domain into 4 equal subdomains for each level in the hierarchy, a quadtree structure was once again used to represent the energies. The energy of a domain is however distributed unevenly on those subdomains, which is the core of the p-model. Starting with an initial eddy of size L_0 and energy E_0, this corresponds to the root node in the eddy quadtree. For each level of the hierarchy, the distribution of energy between the subdomains should be that one half has a fraction $p_1 = 0.7$ distributed equally among them, while the other half has $p_2 = 1 - p_1$. In practice, this is done by drawing

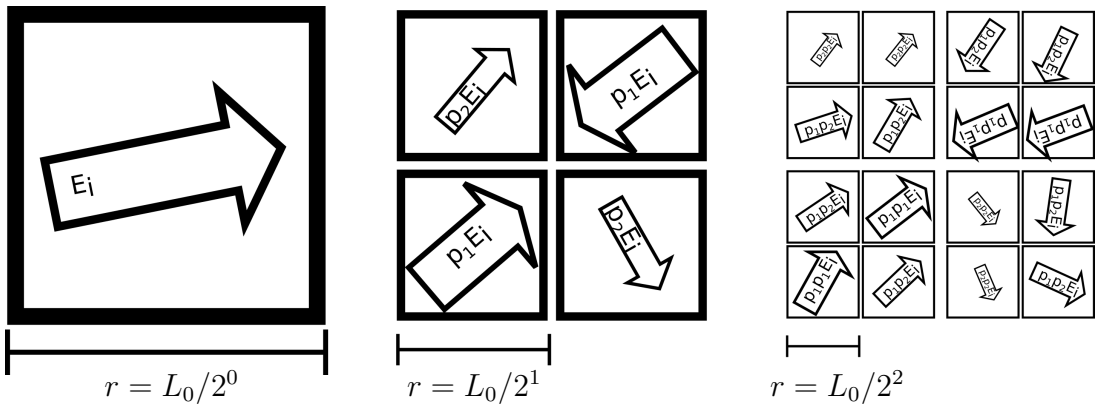

Figure 3.8: Illustration of the iterative generation of eddies in the p-model. This is the two-dimensional equivalent of Figure 2.3 where one considers the turbulent kinetic energy instead of the eddies.

the fractions without replacement, ensuring that the fractions are distributed equally. This is done for all the subsequent divisions of the domain, until one reaches the Kolmogorov scale η for one of the eddies. What was performed in practice was that the number of levels in the hierarchy was rounded to the nearest integer, meaning that it in some cases would not actually be modeled down to η scale, but rather to 2η.

A weakness of this approach is that the number of nodes required for the desired resolution increases as by a factor 4 for each division of the domains. For practical matters, the number of divisions were kept to $l \leq 9$ to ensure a reasonable simulation speed. This means that if one wishes to reach the estimation of the Kolmogorov scale η in resolution, this puts an upper bound on the physical domain one can model turbulence on. In order to still be able to give an estimate of the turbulence for the OD simulations, the turbulence was modeled only for a smaller area, and the entire domain of simulation was mapped to this smaller area to find the effect of the velocity field. It should be noted that this is expected to effect the results, but was done in order to be able to do the simulations in a reasonable time. For the PBC simulations, this was not a problem since one can set the domain size as one wishes in that case.

When initializing the velocity field, only the energy and size of the initial eddy is required. Then divisions are made using the previously stated rules until the length scale is of the order of η. The p-model ensures that the statistical properties of turbulent fluids are preserved, so while the initial velocity field is correct in a statistical sense, it is static. To make the simulation more realistic, a proper time evolution of the turbulent velocity field has been investigated.

3.3.1 Dynamic field

The underlying assumption for the dynamics of the velocity field is that the eddy turnover times govern the main time evolution. It is assumed that the energy of the eddies are determined from the hierarchy of the p-model, so that the energy and length scale for the hierarchy is known for all scales. From equations (2.8) and (2.9), one can thus calculate the eddy turnover time t_l, and use this as a lifetime for the eddy. Using this turnover time, one can then change the eddies once they die out, giving a time evolution of the system. When an eddy dies out, it is assumed that dissipation from the larger eddies ensures that another eddy replaces it, with another direction. In general, these new eddies should be distributed differently (meaning a new draw of ps for the

Table 3.1: The settling times τ of aerosols for unit density spheres in 293 K air. When a particle enters a moving air stream, τ is the time it takes a particle to adopt the velocity of the stream. The table is adapted from page 319 of Seinfeld (1986). Note that the densities of the simulated particles are in general higher, but the table gives a rough estimate.

d_p [µm]	τ [sec]
0.05	4.0×10^{-8}
0.1	9.2×10^{-8}
0.5	1.0×10^{-6}
1.0	3.6×10^{-6}
5.0	7.9×10^{-5}
10.0	3.1×10^{-4}
50.0	7.7×10^{-3}

new eddies) but for simplicity, only the direction of the eddies was changed. These directions are drawn from a uniform random distribution, ensuring that the turbulence in isotropic. This rebirth of eddies happens on all scales, although the smaller eddies have shorter lifetimes and will therefore change more frequently.

3.3.2 Effects on aerosols

When a particle is placed in a turbulent flow, it will in general interact and interfere with the flow as the particle will experience a drag force F_d working along the direction of the flow, as well as impact the pressure in the flow, potentially changing some of the flow properties. The equation (2.13) for the drag force is presented in Section 2.2.3. As the work presented here takes a phenomenological approach, it is not taken into account that the particles may change the pressure of the fluid, and therefore effect the flow. The particles are in that sense ”passive”, as their ability to effect the flow is neglected. This is of course a simplification of the problem, but as long as the densities are relatively low, it is assumed that the effect will be relatively small.

The flow does however effect the aerosols, who very much feel the drag exerted on them. As the BC clusters observed in the atmosphere Scarnato et al. (2015) are relatively small, they are assumed to be so light that they are accelerated to the same velocity as the flow within one time step of the simulation. This is also supported by the calculations done by Seinfeld (1986), where the settling times of unit density spheres at 20 °C in air are calculated for different diameters. The results can be found in Table 3.1, and the numbers support the assumption that the small BC clusters will follow the flow within one time step, depending on the size of the time step. Since the BC particles and clusters are assumed to follow the flow, the conservation of momentum for these light particles is neglected in the simulations.

I addition to the light BC clusters, the larger and heavier mineral dust particles are also exposed to the flow. They are assumed to be so large that they do not follow the flow within one time step, and will thus require a proper investigation of their dynamics in order to simulate their motion. There are several more in-depth studies on this, for instance Guala et al. (2008), which gives a brief introduction to simulation of particle laden flow in turbulence. The approach taken in the work presented here is simpler, in the sense that the pressure is avoided when calculating the force on the particles. As a result, the remaining dominant effect on the particle dynamics is as previously stated the drag force (equation (2.13)). In order to calculate this force, one

needs to know the drag coefficient of spherical particles. This has been studied extensively for instance by Haider and Levenspiel (1989), where the coefficients used were taken from. As all the particles simulated are spherical (at least to an approximation), the drag coefficient for spherical particles $C_D = 0.47$ were used. This is under the assumption that the BC clusters that attach to the dust particles are much smaller than the mineral dust particles themselves. It is also due to the approximation that all mineral dust particles are taken to be spherical to begin with, as an assumption to simplify the numerical implementation. Generally, one should expect the drag coefficient of mineral dust particles to be > 0.47. Once one knows the drag force and the mass of the particles, one may then calculate the acceleration, and thus their displacement as a result of the acceleration during one time step. This dominates the dynamics for larger dust particles, as the diffusion of heavier particles are rather weak in comparison.

3.3.3 Effects on the flow

As the turbulent velocity field is only superimposed and there is no impact from the particles on the flow, this means that one has made an assumption about neglecting the flow passing the particles. Some of the most studied turbulent phenomena are the flow past objects, and it is known that the flow past an object alters the flow. This effect is illustrated in Figure 3.9, where the modeled flow pattern and a more realistic flow pattern is displayed. It is not known whether or not the assumption about neglecting this effect for such small scale particles is justified physically or not, but it is done to keep the model simple. Had the flow been like the situation (b) in Figure 3.9, it is assumed that the lighter BC particles/clusters would, due to their low settling time, be swept passed the particle without colliding, depending on the momentum of the particle, the angle of the motion of the particle, and the angle of the flow. Because of this, one cannot discard the possibility that collisions occur at a lower rate than the model presented in this thesis predicts.

Implementing this effect in the model would require knowledge about the probability of a collision, given the momentum and relative angle between the motion of the particle and the air flow. It could be solved in the narrow phase collision detection with some probability coefficient, but this has not been pursued in this thesis.

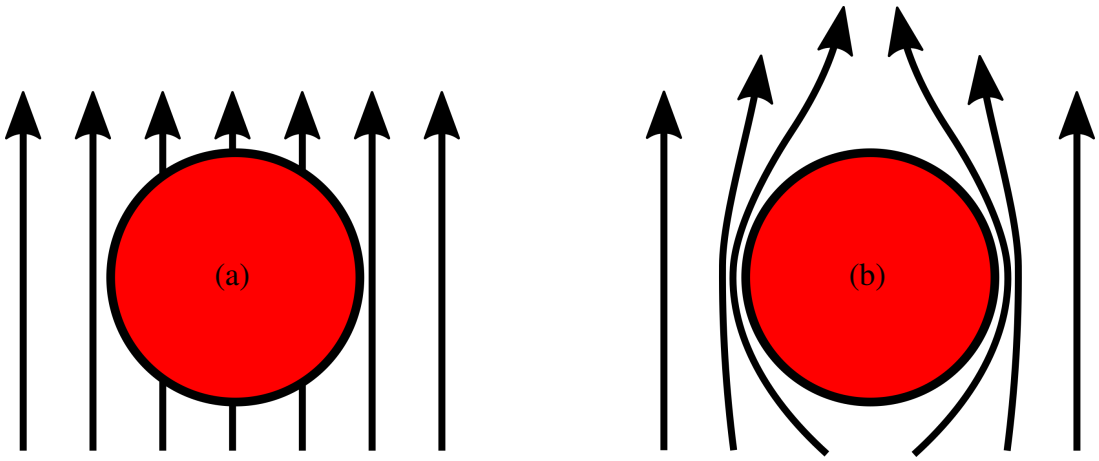

Figure 3.9: The flow pattern past objects as modeled in the simulations (a), and a more realistic flow pattern (b). Although these are depicted as laminar flows, there will in general occur some turbulence as the flow passes the particles. This is however not the interesting point about the flow in this case, as it is the acceleration from passing the particle which will be important for determining if a hit happens. This is as (a) shows neglected for the simulations.

Chapter 4

Results and discussion

The majority of the time at disposal when working on this thesis was spent on the first two aims for the thesis listed in Section 1, which have been described up until this point. Therefore, there was limited time to achieve the last aim, which was to investigate the model that has been developed. There was spent a lot of time testing the model, making sure that every aspect of it was working as intended, but the ultimate test is to try to apply it to the problem of interest, namely the mixing of BC clusters and mineral dust particles. That includes finding the deposition rate which it is hypothesized requires BC clusters to attach to mineral dust particles, which are then deposited. As discussed in Section 3.1.1, there are two main possibilities when simulating the mixing, namely open domain (OD) simulations and periodic boundary conditions (PBC) simulations.

Despite the disadvantages of OD simulations discussed in Section 3.1.1 along with the problems of aerosol concentrations discussed in Section 3.1.2, having a mass gradient in the system originating from a source seems the most relevant given the physical system one tries to simulate. There was therefore initially tested simulations on open domains to determine if this was a suitable approach to take. Later on the periodic boundary system was investigated, and results from the two systems were compared to the extent they were comparable.

Unfortunately, there are too many parameters assumed to have an effect on the mixing to test them all in this thesis. From the results of the project work leading up to this thesis (Berntsen (2015b)), the inspection of the relation between starting concentrations and collisions suggests that the concentrations are a leading factor for the mixing. Thus the first parameters of focus have been the concentrations, which have been investigated balancing the experimentally reported concentrations to the desire of results from simulations run for a limited time.

4.1 Initial open domain testing

For the first simulations, the open system was analyzed in order to determine if one would be able to obtain any significant results. As discussed extensively in Section 3.1.2, the amount of particles in the simulated system is of great importance, and is from experimental observations assumed to be very low. By this, it is meant that it is a very low probability of collisions of BC particles with mineral dust particles with the given concentrations, and it would require very long simulations in order to achieve significant results. To simulate an open system over a physical time long enough to yield significant results, one needs to speed up the simulations

either by using a very coarse time interval (which affects the effective lifetimes of the dust particles), or one must increase the density of particles.

To begin with, the larger time step approach was taken. This is not done completely without loss of generality, as it decreases the resolution for the lifetime τ_{fallout} of the dust particles. The time step was thus chosen so that the effect on particle lifetimes were negligible, while still being as large as possible. Keeping in mind that the situation one is interested in simulating is to have a source of carbon in an open system, it is important to know the number of carbon particles which should be distributed on the domain in order to achieve results comparable to Scarnato et al. (2015). This is also one of the motivations to perform said test simulation. As the radius of BC particles r_{carbon} was assumed to be approximately 10 nm, this value was used initially. Just to set a reference value because the estimate of Section 3.1.2 seemed out of reach, $N_{\text{carbon}} = 10000$ BC particles of size $r_{\text{carbon}} = 10$ nm were used. They were distributed on a square of sides $L_{\text{carbon}} = 0.001$ m within a square of sides $L = 0.5$ m populated with $N_{\text{dust}} = 90$ (corresponding to the more modest peak measurements) dust particles of size $r_{\text{dust}} = 1\ \mu\text{m}$ (see Figure 3.2 for an illustration, although the dust domain is not restricted as much). Simulations were performed for a physical time of $t = 1$ second, with a time step $\Delta t = 5.5 \times 10^{-5}$ s per iteration. The approach taken is to investigate the evolution of the pure BC clusters to get a starting concentration of BC that seems reasonable, in analogy to what was discussed about BC concentrations in Section 3.1.2. What is meant by reasonable is to have a population of clusters which is comparable to what is observed experimentally, while maintaining a tolerable simulation speed. Additionally, a weak turbulent mixing where the largest eddy had an initial turbulent kinetic energy quadratically proportional to $u_0 = 0.18$ m/s was used, corresponding to a Reynolds number $\text{Re} \approx 5000$, which is just above the threshold for turbulent flows. It appears that the results are heavily influenced by the fact that the dust concentration is so low. A summary of the simulation can be found in Figure 4.1.

From Figures 4.1a and 4.1b, one can see that both the largest cluster and the mean cluster size in the system increases very fast to begin with. This is evidence of the effects of having a high initial carbon concentration discussed in Section 3.1.2, and is what is expected for the behavior of a system with a source. It is also expected that this rate of growth is not sustainable over time, which causes the curves in Figures 4.1a and 4.1b to flatten. The more interesting results of Figures 4.1c and 4.1d does however confirm the suspicion that an open system would be difficult to simulate to get significant results, especially for short simulation times.

Thus the results shown in Figure 4.1 represents a challenge in the sense that one needs to run simulations over longer physical time in order to get significant results. Like discussed earlier, one cannot increase the time steps any more, as this will interfere with the resolution of the lifetimes of the dust particles. Increasing the simulation time would also increase the possible range the carbon particles may move, which will in turn force an increase of the system size in the simulations. As a result, the carbon particles may move outside the domain populated by dust particles, which means they would be in a domain where no interesting mixing can happen. Another possibility is to increase the area populated by dust particles, which as a consequence also must increase the number of dust particles. The main problem with this is that the physical time simulated would require a so large amount of dust particles that the simulations for one time step would take too long to perform. This is a direct result of the inferior scaling of quadtrees with respect to objects in the system, which was discussed in Section 3.2.1. If one increases the total domain areas without increasing the dust population area, one would not only have an unphysical system, but the collisions would not happen due to the BC particles moving in empty space once they leave the area populated by dust.

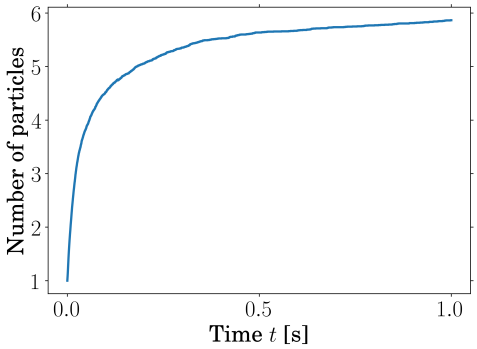

(a) The mean size of the clusters in the simulated system. It is expected to increase rapidly to begin with before it stabilizes after some time.

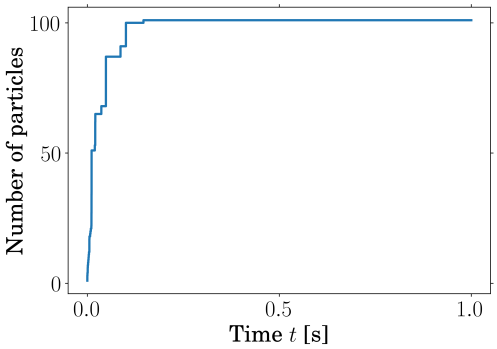

(b) The size of the largest cluster in the system. Like for the mean cluster size, it is expected that the carbon particles rapidly form relatively large clusters due to their high initial concentration before they are diluted and the effect fades.

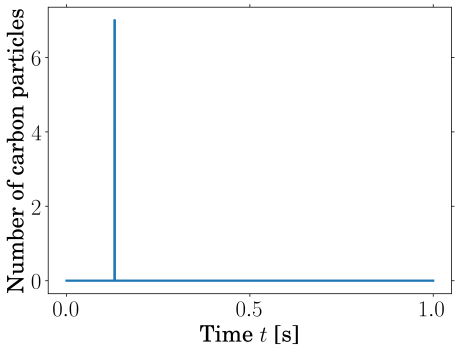

(c) Number of carbon particles attached to a cluster consisting of at least one dust particle. In other words, number of carbon particles which are set to fall out, at a given point in time.

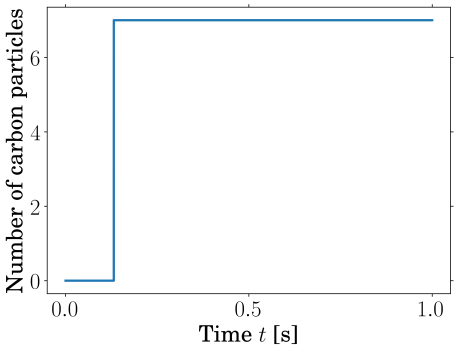

(d) The cumulative amount of carbon particles that has fallen out of the plane.

Figure 4.1: Results for the test simulation of $t = 1$ s performed on an OD system with parameters trying to resemble the physical conditions of the system. The high concentration of the carbon particles makes the short time behavior of them more prominent than the few dust particles. The results also show very little agglomeration of BC particles on mineral dust particles as a results of the mixing.

In an attempt to circumvent this, several simulations with a higher amount of carbon particles (but with a lower "local" BC concentration to avoid the formation of too large clusters) were performed. As mentioned earlier, there is a certain freedom when choosing this concentration, as simulating a physically realistic amount from the source would be impractical (see Section 3.1.2). Therefore one tries to replicate the results with fewer particles form a non-continuous source. The results of a simulation with $N_{\text{carbon}} = 20000$ BC particles of size $r_{\text{carbon}} = 10$ nm distributed on a square of sides $L_{\text{carbon}} = 0.002$ m are presented in Figure 4.2. Once again the total domain has sides $L = 0.5$ m populated with $N_{\text{dust}} = 90$ dust particles of size $r_{\text{dust}} = 1$ μm. The largest scale eddy to simulate the turbulence was given a velocity of $u_0 = 0.18$ m/s to keep the turbulence as before. Unfortunately, the amount of collisions between BC and dust is even lower than for fewer carbon particles. The time step was as in the previous simulation $\Delta t = 5.5 \times 10^{-5}$ s. Although the concentration in total was higher, the initial concentration when distributing the particles were lower due to them being distributed on larger domain. This can bee seen in both Figure 4.2a and 4.2b, where the increase is slower than the previous simulation, and the value at which the increase flattens out is significantly lower. It should also be pointed out that there is a very high uncertainty in these results, especially in the collision rate between BC and mineral dust. The results should therefore only be used qualitatively to see if one can expect anything to happen at all due to the low simulation time and the fact that this is ultimately based on the statistics of the system, which means the results should ideally also be seen in a statistical sense. Since the point of running them in the first place was to see if it would increase the number of BC particles falling out, it appears that increasing the concentration did not significantly alter the results for short time simulations.

Comparing the mean cluster size with the results reported in Figure 1 of Scarnato et al. (2015), it seems apparent that the clusters generated by the simulations are too small. It should also be noted that one does not observe too large BC clusters attached to mineral dust, which suggests that just increasing the distribution concentration of BC is not the way to obtain results comparable to observations. A solution to this problem would be to instead of initializing the BC as single particles, one could initialize the BC as clusters following the size measurements and distributions that have already been observed. An example of such a study is Clarke et al. (2004), however this is not done for the same geographical region as the one this thesis is interested in. It does nevertheless provide a valuable indication of the size distribution of BC clusters, which can serve as a reference value for initial tests. It is thought that this will increase the rate of deposition, although it probably would not change the number of collisions by a significant amount. This should be investigated when improving the model, and it is assumed that modeling a source of BC particles yields inferior results compared to modeling a source of BC clusters.

It is also possible to assume that the concentration of dust particles may locally be higher than what is reported. It is pointed out by Ryder et al. (2013) that heavy dust particles are only found in altitudes up to ≈ 1 km, and it is argued that most measurements are not done close to the sources of the dust. In a study done by Rosen (1964), the vertical profile of aerosols are presented, which supports the assumption that the density of aerosols may be higher closer to the surface. Between the usual altitudes of measurement being higher than the usual height of a gas flare on a well, and the measurements not necessarily being in the source regions for the mineral dust, experimenting with higher mineral dust concentrations seems justifiable. As one is already using the peak measurement values for the concentration of the mineral dust, it should be pointed out the main motivation for increasing the number is still not strictly physical. It is rather done to be able to see evidence of the BC falling out due to attachment to mineral dust,

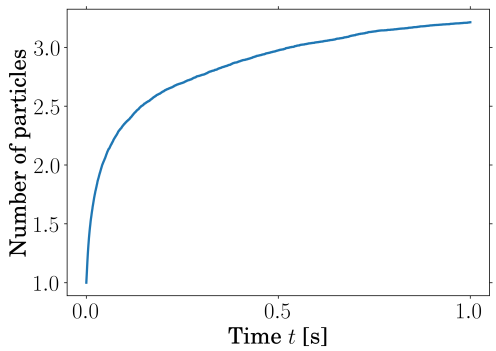

(a) The mean size of the clusters in the simulated system. It is expected to increase rapidly to begin with before it stabilizes after some time.

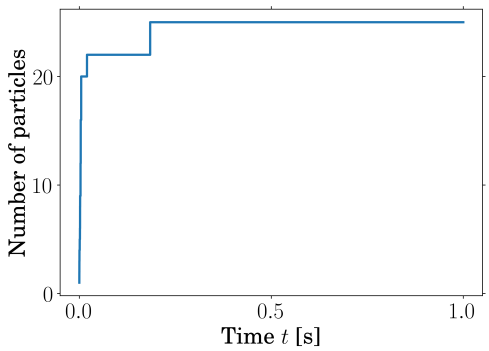

(b) The size of the largest cluster in the system. Like for the mean cluster size, it is expected that the carbon particles rapidly form relatively large clusters due to their high initial concentration before they are diluted and the effect fades.

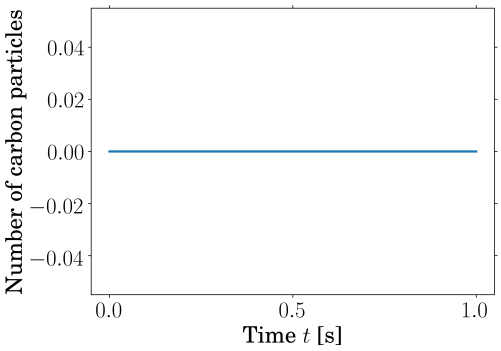

(c) Number of carbon particles attached to a cluster consisting of at least one dust particle. In other words, number of carbon particles which are set to fall out, at a given point in time.

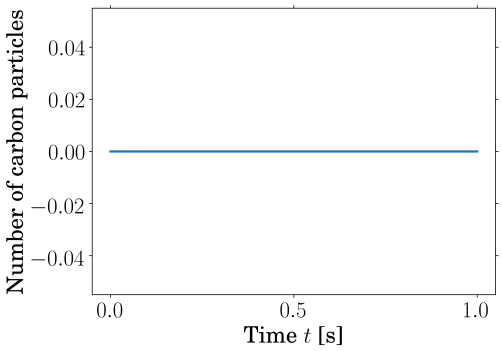

(d) The cumulative amount of carbon particles which has fallen down.

Figure 4.2: Results for a simulation of $t = 1$ s for an open domain where the concentration C_{carbon} was doubled. The total amount of BC $N_{\text{carbon}} = 20000$ particles was used, in order to check if an increase in C_{carbon} would be significant for the deposition rate.

which is what one tries to model even when simulating short times.

To obtain these higher concentrations would require whirling of mineral dust from the surface due to strong winds (see Gillette et al. (1974)), which is a problem with respect to the simulations of turbulence. This problem has already been described in Section 3.3, and the implication is dropped in the following. In other words the simulations were done using the same turbulence modeling as for the previous runs, while still having a higher concentration of mineral dust.

The results of a simulation of $N_{\text{carbon}} = 10000$ BC particles of $r_{\text{carbon}} = 10$ nm distributed on a square of sides $L_{\text{carbon}} = 0.001$ m with a concentration of 360 dust particles of size $r_{\text{dust}} = 1$ μm distributed on square of sides $L = 0.5$ m, simulated for $t = 1$ second is presented in Figure 4.3. Time step and turbulence parameters are as in the previous simulations. Figure 4.3a has a behavior similar to previously presented results, with the exception of a noticeable dip at $t \approx 0.34$ s. This is explained in Figure 4.3c, where one can see that a relatively large BC cluster fell out at the specified time. Additionally, one sees from Figure 4.3c and 4.3d that there are several events where carbon fell from the system during the simulations. Although other simulations of the same system did not have as many collisions between BC and mineral dust as the simulation presented in Figure 4.3, the sensitivity of deposition rate with respect to initial concentration is clear. With a higher amount of dust in the system, there is a higher rate of collisions with BC clusters, and therefore more BC falling out of the plane.

From the results presented up to this point, it seems clear that to get more reliable results, one has to simulate longer times, which means that one has to use PBC to avoid the problems arising in the OD simulations. Even then, one cannot guarantee the validity of the results due to the variance displayed in the results presented up until now.

4.2 Periodic boundary conditions simulations

With periodic boundary conditions, one is able to perform simulations without having to worry about particles leaving the domain. This simplifies the turbulence modeling because one may now limit the domain of turbulence, which in turn helps with the resolution problem described in Section 3.3. It also solves the problem of particles leaving the domain as they could do for open systems, meaning that there is now no practical upper bound for simulation times.

To see if there was any effect in allowing the system to mix longer, simulations were run using $N_{\text{carbon}} = 20000$ BC particles of $r_{\text{carbon}} = 10$ nm initially distributed on a square of sides $L_{\text{carbon}} = 0.002$ m with a concentration of 360 dust particles of size $r_{\text{dust}} = 1$ μm distributed on a square with sides $L = 1$ m, simulated for $t = 10$ seconds with $\Delta t = 5.5 \times 10^{-5}$ s. The largest scale eddy to simulate the turbulence was given a velocity of $u_0 = 0.18$ m/s. Results from one of the simulations performed are shown in Figure 4.4.

Apart from the obvious increase in total accumulated carbon on dust particles, there are several other interesting results in Figure 4.4. It seems evident from Figure 4.4a that even with a slightly higher initial concentration of BC and longer simulation time, the mean cluster size is still smaller than one had expected from the observation of Scarnato et al. (2015). An additional (although in practice negligible) problem related to this is that once the BC particles are deposited, they are re-introduced as single particles within the original BC domain L_{carbon}. This is something that one could accommodate by instead of reintroducing BC particles to the system as single BC particles, they could be part of BC clusters to begin with, as discussed previously.

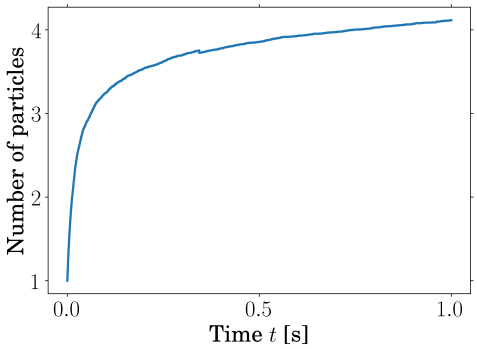

(a) The mean size of the clusters in the simulated system. It is expected to increase rapidly to begin with before it stabilizes after some time.

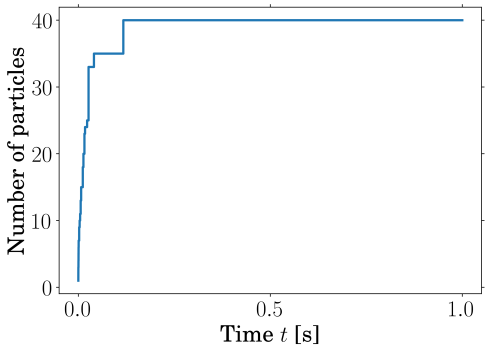

(b) The size of the largest cluster in the system. Like for the mean cluster size, it is expected that the carbon particles rapidly form relatively large clusters due to their high initial concentration before they are diluted and the effect fades.

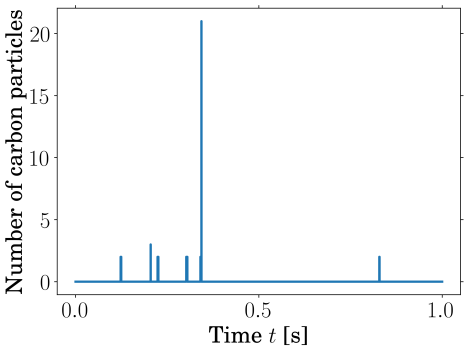

(c) Number of carbon particles attached to a cluster consisting of at least one dust particle. In other words, number of carbon particles which are set to fall out, at a given point in time.

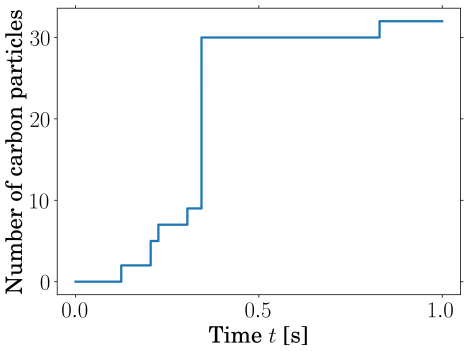

(d) The cumulative amount of carbon particles which has fallen down.

Figure 4.3: Results for a simulation of $t = 1$ s for an open domain where the concentration C_{dust} was increased to 1440 particles/m^2. This was done to see the impact a change in dust concentration C_{dust} would have on the deposition rate.

Another interesting result is displayed in Figures 4.4c and 4.4d where one can see that after one second of simulating, there had not been any carbon falling out. This is comparable to the results presented in Figure 4.2, where no collision between carbon and mineral dust happened. It indicates that in order to achieve significant results, one should perform as long simulations as possible and calculate the deposition rate based on these. This is another argument for why the PBC simulations are superior to the OD simulations for this system. It also to some extent confirms the assumption that the BC will latch to mineral dust particles after a short time (compared with the typical timescales for particles in the atmosphere). One should still be careful about the exact numbers and rates, and rather focus on the fact that the model gives results where collisions do occur.

Unfortunately, there was a limited time available to perform these simulations for as long as one would have liked. Based on the results obtained by the simulations run this far, it was deemed that one would not be able to achieve significant results with the concentrations found from experimental studies. This is not to say that it would be impossible to achieve these results with the model proposed in this thesis, but rather that one should not waste the time at disposal by being overly focused on one thing. Even though the simulations with observed concentration arguably yields the most interesting results, there are other things to investigate about the model.

4.2.1 Implications

If one assumes that the rate of dissipation is correct, there are some implications to the deposition and evolution of N_{carbon}. If one neglects the reintroduction of BC particles in the model and the dependence it has on the deposition, it is possible to estimate how long it would take to deplete the area for BC particles, estimating a total lifetime for them. For a given concentration of dust particles and turbulent mixing state of the air, one can assume that the loss of BC particles by deposition on the dust particles are first order, i.e. proportional to the concentration of BC particles (N_{carbon}). The rate of change of N_{carbon} is then given by

$$\frac{\mathrm{d}N_{\text{carbon}}}{\mathrm{d}t} = -lN_{\text{carbon}}, \tag{4.1}$$

where l is the loss rate depicted by the model, which based on Figure 4.4 is

$$\frac{\frac{63\,\text{particles}}{20000\,\text{particles}}}{10\,\text{s}} = 3.15 \times 10^{-4}\text{s}^{-1}, \tag{4.2}$$

then the solution to (4.1) is

$$N_{\text{carbon}}(t) = N_{\text{carbon}}(t_0)e^{-lt}. \tag{4.3}$$

The lifetime is defined as the e-folding time (in this case for BC particles with respect to being attached to a dust particle) $\tau_{\text{BC}} = \frac{1}{l}$, which when one inserts the numbers gives $\tau_{\text{BC}} \approx 53$ minutes. In other words, in this experiment it would take less than 1 hour for 63 % of the BC particles to attach to mineral dust particles, which means that deposition in the areas close to the source of BC seems reasonable. Due to the stochastic nature of the model, the estimate from (4.2) is quite uncertain. To reduce this uncertainty, one can either have longer simulations (like already suggested) or have an ensemble of shorter simulations. The simulation times

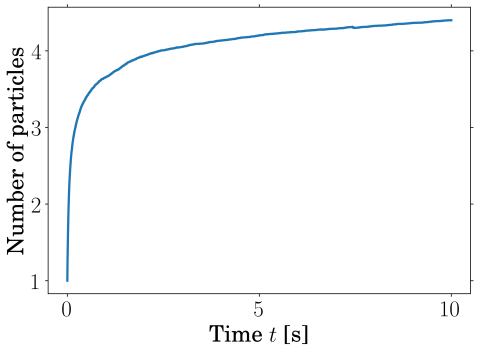

(a) The mean size of the clusters in the simulated system. It expected to increase rapidly to begin with before it stabilizes after some time.

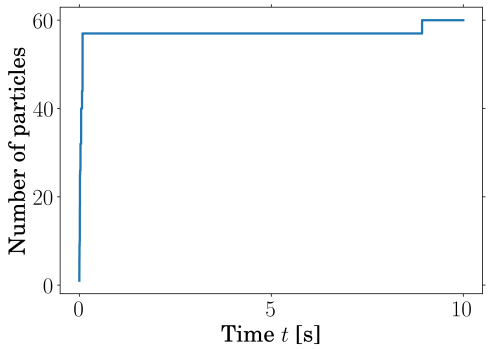

(b) The size of the largest cluster in the system. Like for the mean cluster size, it is expected that the carbon particles rapidly form relatively large clusters due to their high initial concentration before the are transported.

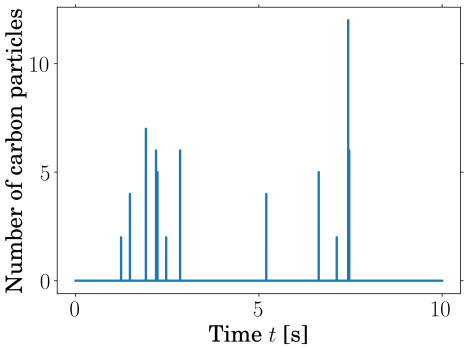

(c) Number of carbon particles attached to a cluster consisting of at least one dust particle. In other words, number of carbon particles which are set to fall out, at a given point in time.

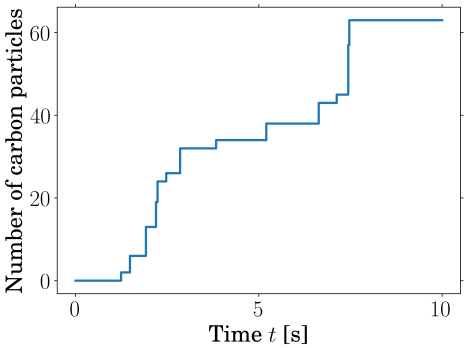

(d) The cumulative amount of carbon particles which has fallen down.

Figure 4.4: Results for the simulation of $t = 10$ s with periodic boundary conditions. The parameters for this simulation were chosen so that the simulated system resembles what has been measured. Even though the results are not very different from the OD simulations in terms of deposition rate, one now has a better basis for the determining the rate.

will as already suggested be very dependent on the mineral dust concentration. Nevertheless with these quite rough estimates, the results from the model support the hypothesis that there could be significant BC deposition in the desert areas described in Chapter 1. Note that the lifetime is dependent on the concentration of mineral dust particles, but independent on the concentration of BC. This is due to the lifetime for BC being determined by the probability of that BC to collide with any mineral dust particle. Decreasing the BC concentrations in the simulations would require longer simulations to get a statistically robust result, however the estimated lifetime should be the same. It would most certainly require more than $\tau_{\text{BC}} \approx 53$ minutes (which is estimated for a case with high dust concentrations) to transport the BC far from the source, depending on wind speed. The wind direction would usually also determine if the BC is transported to be deposited over the ocean, or if it will be deposited over land. The important thing is still that the rate the model predicts (however uncertain) will most likely give deposition of a major fraction of the BC emitted within the desert regions with high surface albedo. This means that the BC could have a climate impact by changing the surface albedo.

4.3 Investigations of dust concentration dependence

As was mentioned in the beginning of Chapter 4, the only deeper investigation was done on the effect the concentration of mineral dust particles in the system would have on the deposition rate. With the same arguments as before with respect to what range of concentration one is interested in, the lower bound of the concentration range investigated was set to 200 particles/m^2, corresponding to about twice the concentration of the median values reported by Marticorena et al. (2010).

The radius of the BC particles has up until this point been assumed to be $r_{\text{carbon}} = 10$ nm due to that being the approximate order of their size. According to sources like Kravitz et al. (2012), there could be BC particles with radius larger than this. Therefore, the radius was doubled to $r_{\text{carbon}} = 20$ nm, as was suggested by Scarnato et al. (2015). This could effect the collision rate as the particles now occupy a larger part of space. There will however not be done an in-depth study of the relation between radius (size) and deposition rate for neither BC nor mineral dust particles.

The results of the dust concentration investigations were all obtained using PBC and $t = 10$ s simulation time with time steps of $\Delta t = 5.5 \times 10^{-5}$ s. In order to understand the dependence on the dust concentration, simulations were run for $C_{\text{dust}} \in [200, 2000]$ particles/m^2 with steps of 200 particles/m^2. This corresponds to approximately $c_{\text{dust}} \in [1.68 \times 10^{-8}, 1.68 \times 10^{-7}]$ µg/m^2. The parameters for the simulations are listed in Table 4.1, and are for the most part similar to the previously run simulations. Unfortunately, the simulations were interrupted by a power outage [1]. The results are presented in Figure 4.5, where the relation between the deposition rate and C_{dust} is reported. From Figure 4.5, one can see that there are several deviations from the expected increase in deposition rate as C_{dust} increases. This is assumed to be due to the uncertainties stemming from the limited time available to run each simulation. By only being able to simulate a very limited time, one should be careful not to trust these results too much in a quantitative sense. It also seems unwarranted to include any sort of trend line in the plot, as

[1] There was a power outage in the city of Trondheim, which killed all the simulations a little over a week before the deadline for the thesis. It was not possible to continue those simulations, so they were restarted. Unfortunately, there was therefore not enough time to let them all run for as long as one may have wished. The final simulations were ended mere hours before the deadline.

Table 4.1: Table of some of the main parameters for the concentration investigations. Omitted from the table is u_0, which has been kept at the same value as before for all the simulations. Note that the simulation times are done for different times t since there was a power outage when running the simulations. This power outage meant that the simulations for higher mineral dust concentrations would not be completed withing the deadline for the thesis. The rates in Figure 4.5 are therefore based on simulations run with different times, which is unfortunate.

r_{carbon} [m]	r_{dust} [m]	N_{carbon} [particles]	L [m]	L_{carbon} [m]	C_{dust} [particles/m^2]	t [s]
20×10^{-9}	1.0×10^{-6}	20 000	1.0	0.001	200	10.0
20×10^{-9}	1.0×10^{-6}	20 000	1.0	0.001	400	10.0
20×10^{-9}	1.0×10^{-6}	20 000	1.0	0.001	600	10.0
20×10^{-9}	1.0×10^{-6}	20 000	1.0	0.001	800	10.0
20×10^{-9}	1.0×10^{-6}	20 000	1.0	0.001	1000	9.02
20×10^{-9}	1.0×10^{-6}	20 000	1.0	0.001	1200	7.74
20×10^{-9}	1.0×10^{-6}	20 000	1.0	0.001	1400	6.75
20×10^{-9}	1.0×10^{-6}	20 000	1.0	0.001	1600	5.95
20×10^{-9}	1.0×10^{-6}	20 000	1.0	0.001	1800	5.44
20×10^{-9}	1.0×10^{-6}	20 000	1.0	0.001	2000	4.89

the results are so deviating. With that being said, one could make the argument that there will be more deviations for the simulations with higher dust concentrations, which could explain why there is a such a gap between the rates for $C_{\text{dust}} = 1800$ particles/m^2 and $C_{\text{dust}} = 2000$ particles/m^2. Once again, it is argued that either longer simulations or having a larger ensemble would be a solution for this.

In spite of this uncertainty and the deviations, the results of Figure 4.5 are uplifting for the model, and for the hypothesis requiring attachment of BC to mineral dust for deposition to happen. Everything in the model appears to be working as intended, and the fact that it gives definite results that collisions between BC clusters and mineral dust particles occur gives strong support for the initial hypothesis. This indicates that there may be some initial deposition of BC close to the sources. The model could in that sense be deemed a success, even though it as discussed extensively has weaknesses, and some caution should be taken when looking at the results.

Due to the problem of the observed carbon clusters attached to the mineral dust particles being larger than what the model gives, there is good reason to be skeptic about the deposition rates reported in Figure 4.5. Although the model predicts some downfall, it has not been possible to find any studies that reports the concentration of BC on the surface of the areas of interest to confirm the results from the model. Therefore, one cannot at this point in time give a proper evaluation of the model, specifically for the problem in mind.

Neither have the attempts to find any other studies looking at the mixing rate of BC particles/clusters and mineral dust particles been successful. To properly evaluate the model, it seems reasonable to start in the atmosphere where the mixing happens. It would therefore also require an experimental study of the mixing in the atmosphere close to the BC source. This could for instance be achieved by comparing the upstream and downstream concentrations of BC around a source like a gas flare.

As mentioned in the beginning of this chapter, there has not been enough time to perform all the simulations that one would have wished to perform. There has also not been time to perform the simulations for as long time as one would have liked. Some words about the wall

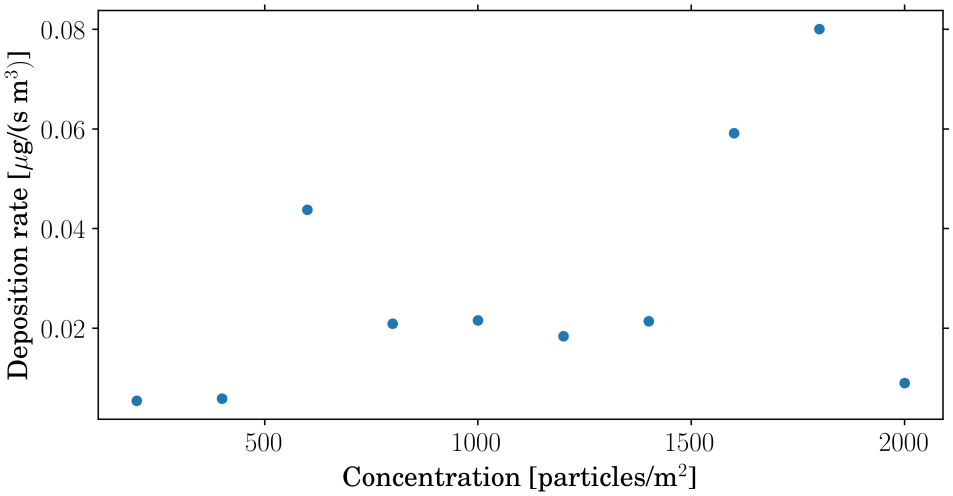

Figure 4.5: The deposition rate of BC as a function of mineral dust concentration in the system for parameters stated in Table 4.1.

time of the simulations are therefore in order. The typical wall time of the simulations has been related to both the time steps and the number of dust particles. For the dependence on Δt, it is quite obvious that a smaller time step will require more iterations, and therefore a longer wall time. The dependence on number of dust particles is more subtle, but is partially due to the fact that the redistribution routine for the particles falling out is relatively slow, and it was not done any effort to speed this up. Another cause of the poor scalability with respect to mineral dust particles is the choice of container for the clusters, which is not very efficient when removing clusters. This was chosen at the beginning, and there was no problem with this until the simulations were run for long times t, at which point there was not enough time to go back and change this to improve the scalability. There are therefore rather large differences in wall times for the different simulations, mostly depending on C_{dust} and the time t simulated. The simulations for $t = 10$ s with $C_{\text{dust}} = 200$ particles in Figure 4.5 took ≈ 70 hours to complete. The similar simulations of $C_{\text{dust}} = 800$ particles took ≈ 171 hours. If the code is left as-is, one would therefore require quite a long time to obtain statistically significant results for the concentrations in Figure 4.5. Estimating the wall time is hard, as the time required per iteration increases as the simulation runs. A rough estimate is that one would be able to simulate $t = 60$ s with concentrations in the range which has been observed in approximately one month wall time. It should be pointed out that simulations were run on i7 CPU 960 3.20GHz processors (single thread), and were not parallelized to run on a supercomputer.

When looking at the results the model developed has been able to produce, there are several things to consider. To begin with, there are still many parameters that are uncertain. Some of these could be approximated theoretically, but other requires experimental results to improve the estimates used in this thesis. The difficulty of simulating a two-dimensional system with turbulence which is intended to represent a three-dimensional physical world is one of the things suggesting that expanding the model to three dimensions would be beneficial. That would resolve the problem of two-dimensional turbulence, but impose a new problem when simulating three-dimensional turbulence numerically as the simulation is slow and requires a lot of RAM even for the two-dimensional case presented here. A possible way of improving the model is

to further investigate the method for modeling the motion of particles in turbulence proposed in Section 2.3 which would eliminate the RAM problem.

There are also several physical effects that one should try to include in the model. The particles are strictly passive in the simulations done in this thesis, but as discussed in Section 3.3.2, they would in general effect the pressure of the fluid, meaning that the particles could also effect the flow of the fluid. One should therefore take what was discussed in Section 3.3.3 about the flow around the particles themselves into account.

The reason why so many of these improvements to the model was not implemented in the first place was that the main idea was to keep the model as simple as possible. By creating a simple model to begin with, one is able to expand and build on the simple model as one slowly gets closer to resembling the physical world. Most of the decision about what algorithms/methods to use were taken keeping this idea of keeping simple in mind. There may yet be simpler ways to achieve what has been achieved in this thesis, but with the philosophy of keeping things simple and moving forward with them has ensured stable progress from beginning to the end of developing the model.

Chapter 5

Conclusion and outlook

5.1 Conclusion

In this thesis some of the driving mechanisms for mixing, agglomeration, and deposition of BC and mineral dust particles have been presented. A method for simulating a two-dimensional system with said mixing and deposition has been developed and studied. When presented with more than one possible way of solving a problem, the reasons for choosing the methods/algorithms have been presented and discussed, and the choices of methods/algorithms have been evaluated. Although it is a very ambitious task to be able to simulate a physical system of both particle collisions and turbulence, the model that has been presented yields results, although obtaining statistically significant results would require more time than was available when working on this thesis. The model is not only useful for the system discussed in this thesis, but can generally be used for many mixing processes and problems of modeling agglomeration.

5.2 Outlook

Throughout the thesis, several improvements to the model have been suggested and discussed. Some of them may not improve the model significantly, but are still small improvements. That is symptomatic for the model, where it can be improved in many areas but has been formed with the philosophy of keeping it simple.

Like stated in Section 4.3, there has been no success in finding any studies reporting neither the mixing rates, nor the deposition rates of BC as observed experimentally. This does not come as a surprise, as it appears that the hypothesis presented in Chapter 1 appears to be new. Some observational studies are therefore recommended both to evaluate the model, and verify the results it predicts. It would seem natural to start in the atmosphere like suggested in Section 4.3, but also to investigate the BC after it has been deposited. This would include experimental observations of both the deposition rate of BC in addition to studying the amount of BC found in desert areas today. That work would require a method for distinguishing and filtering the BC from the other particles present in the soil, which can be challenging. When investigating the amount of BC in the soil, this also raises the question of what happens to the BC once it has been deposited. As wind whirl up the dust particles, it seems reasonable to assume that this will also happen to the carbon, which suggests that there are still quite a distance to go before the life-cycle of BC and the effect it has in desert areas is fully understood. Some experimental

data to compare the model to seems necessary to improve it, to have some idea of where it is inaccurate or insufficient.

In addition to do experimental studies to put the hypothesis (and thus the model) to the ultimate test, there are still several things to improve on the model itself. Even with the model as it is at this point in time, there are several parameters that could be either altered or given better estimates to improve the results. It is however hard to identify what should be improved in the model without having any experimental data to compare with. If it turns out that observations are made at some point, and the results predicted by this model is in poor agreement with these, one could update the model to include some of the physical effects mentioned throughout this thesis that has not been implemented at this stage. Any observations would hopefully indicate what these improvements might be.

Bibliography

Alpert, P., Ganor, E., 2001. Sahara mineral dust measurements from toms: Comparison to surface observations over the middle east for the extreme dust storm, march 1417, 1998. Journal of Geophysical Research: Atmospheres 106 (D16), 18275–18286.
URL http://dx.doi.org/10.1029/2000JD900366

Berntsen, S., 2015a. Master thesis code. https://github.com/berntsim/masters.

Berntsen, S., December 2015b. Modeling agglomeration of aerosols. Project thesis, NTNU - Norwegian University of Science and Technology, Høgskoleringen 5, Realfagbygget D5-170.

Bohr, T., Jensen, M. H., Paladin, G., Vulpiani, A., 1998. Dynamical Systems Approach to Turbulence. Cambridge University Press, cambridge Books Online.
URL http://dx.doi.org/10.1017/CBO9780511599972

Bond, T. C., Doherty, S. J., Fahey, D. W., Forster, P. M., Berntsen, T., DeAngelo, B. J., Flanner, M. G., Ghan, S., Krcher, B., Koch, D., Kinne, S., Kondo, Y., Quinn, P. K., Sarofim, M. C., Schultz, M. G., Schulz, M., Venkataraman, C., Zhang, H., Zhang, S., Bellouin, N., Guttikunda, S. K., Hopke, P. K., Jacobson, M. Z., Kaiser, J. W., Klimont, Z., Lohmann, U., Schwarz, J. P., Shindell, D., Storelvmo, T., Warren, S. G., Zender, C. S., 2013. Bounding the role of black carbon in the climate system: A scientific assessment. Journal of Geophysical Research: Atmospheres 118 (11), 5380–5552.
URL http://dx.doi.org/10.1002/jgrd.50171

Buras, R., Dowling, T., Emde, C., 2011. New secondary-scattering correction in disort with increased efficiency for forward scattering. Journal of Quantitative Spectroscopy and Radiative Transfer 112 (12), 2028–2034.

Cantor, G., 1883. Ueber unendliche, lineare punktmannichfaltigkeiten. Mathematische Annalen 21 (4), 545–591.
URL http://dx.doi.org/10.1007/BF01446819

Clarke, A. D., Shinozuka, Y., Kapustin, V. N., Howell, S., Huebert, B., Doherty, S., Anderson, T., Covert, D., Anderson, J., Hua, X., Moore, K. G., McNaughton, C., Carmichael, G., Weber, R., 2004. Size distributions and mixtures of dust and black carbon aerosol in asian outflow: Physiochemistry and optical properties. Journal of Geophysical Research: Atmospheres 109 (D15), n/a–n/a, d15S09.
URL http://dx.doi.org/10.1029/2003JD004378

Dahlback, A., Stamnes, K., 1991. A new spherical model for computing the radiation field available for photolysis and heating at twilight. Planetary and Space Science 39 (5), 671–683.

Eden, M., 1961. A two-dimensional growth process. In: Proceedings of the Fourth Berkeley Symposium on Mathematical Statistics and Probability, Volume 4: Contributions to Biology and Problems of Medicine. University of California Press, Berkeley, Calif., pp. 223–239.
URL http://projecteuclid.org/euclid.bsmsp/1200512888

Einstein, A., 1905. Investigations on the theory of the brownian movement. Ann. der Physik.
URL http://www.physik.fu-berlin.de/~{}kleinert/files/eins_brownian.pdf

Elvidge, C. D., Zhizhin, M., Baugh, K., Hsu, F.-C., Ghosh, T., 2016. Methods for global survey of natural gas flaring from visible infrared imaging radiometer suite data. Energies 9 (1), 14.
URL http://www.mdpi.com/1996-1073/9/1/14

Ericson, C., 2004. Real-Time Collision Detection. CRC Press, Inc., Boca Raton, FL, USA.

Evans, L., 2010. Partial Differential Equations. Graduate studies in mathematics. American Mathematical Society.
URL https://books.google.no/books?id=Xnu0o_EJrCQC

Flagan, R. C., Seinfeld, J. H., 1988. Fundamentals of air pollution engineering.

Flanner, M. G., Zender, C. S., Hess, P. G., Mahowald, N. M., Painter, T. H., Ramanathan, V., 2009. Springtime warming and reduced snow cover from carbonaceous particles. Atmospheric Chemistry and Physics 9 (7), 2481 – 2497.
URL http://escholarship.org/uc/item/2gw2j3bs

Forster, P., Ramaswamy, V., Artaxo, P., Berntsen, T., Betts, R., Fahey, D. W., Haywood, J., Lean, J., Lowe, D. C., Myhre, G., et al., 2007. Changes in atmospheric constituents and in radiative forcing. chapter 2. In: IPCC (Ed.), Climate Change 2007. The Physical Science Basis. IPCC, pp. 129–234.

Frisch, U., Kolmogorov, A., 1995. Turbulence: The Legacy of A. N. Kolmogorov. Cambridge University Press.
URL https://books.google.no/books?id=K-Pf7RuYkf0C

Frisch, U., Parisi, G., 1985. Fully developed turbulence and intermittency. Turbulence and predictability in geophysical fluid dynamics and climate dynamics.

Frisch, U., Sulem, P.-L., Nelkin, M., 8 1978. A simple dynamical model of intermittent fully developed turbulence. Journal of Fluid Mechanics 87, 719–736.
URL http://journals.cambridge.org/article_S0022112078001846

Gillette, D. A., Blifford, I. H., Fryrear, D. W., 1974. The influence of wind velocity on the size distributions of aerosols generated by the wind erosion of soils. Journal of Geophysical Research 79 (27), 4068–4075.
URL http://dx.doi.org/10.1029/JC079i027p04068

Guala, M., Liberzon, A., Hoyer, K., Tsinober, A., Kinzelbach, W., 2008. Experimental study on clustering of large particles in homogeneous turbulent flow. Journal of Turbulence (9), N34.

Haider, A., Levenspiel, O., 1989. Drag coefficient and terminal velocity of spherical and nonspherical particles. Powder Technology 58 (1), 63 – 70.
URL http://www.sciencedirect.com/science/article/pii/0032591089800087

Halsey, T. C., Jensen, M. H., Kadanoff, L. P., Procaccia, I., Shraiman, B. I., Feb 1986. Fractal measures and their singularities: The characterization of strange sets. Phys. Rev. A 33, 1141–1151.
URL http://link.aps.org/doi/10.1103/PhysRevA.33.1141

Hansell Jr., R. A., Reid, J. S., Tsay, S. C., Roush, T. L., Kalashnikova, O. V., 2011. A sensitivity study on the effects of particle chemistry, asphericity and size on the mass extinction efficiency of mineral dust in the earth's atmosphere: from the near to thermal ir. Atmospheric Chemistry and Physics 11 (4), 1527–1547.
URL http://www.atmos-chem-phys.net/11/1527/2011/

Hansen, J., Nazarenko, L., 2004. Soot climate forcing via snow and ice albedos. Proceedings of the National Academy of Sciences of the United States of America 101 (2), 423–428.
URL http://www.pnas.org/content/101/2/423.abstract

Haywood, J. M., Shine, K. P., 1995. The effect of anthropogenic sulfate and soot aerosol on the clear sky planetary radiation budget. Geophysical Research Letters 22 (5), 603–606.
URL http://dx.doi.org/10.1029/95GL00075

Huang, K., Fu, J. S., Prikhodko, V. Y., Storey, J. M., Romanov, A., Hodson, E. L., Cresko, J., Morozova, I., Ignatieva, Y., Cabaniss, J., 2015. Russian anthropogenic black carbon: Emission reconstruction and arctic black carbon simulation. Journal of Geophysical Research: Atmospheres 120 (21), 11,306–11,333, 2015JD023358.
URL http://dx.doi.org/10.1002/2015JD023358

Koch, D., Del Genio, A. D., 2010. Black carbon semi-direct effects on cloud cover: review and synthesis. Atmospheric Chemistry and Physics 10 (16), 7685–7696.
URL http://www.atmos-chem-phys.net/10/7685/2010/

Kravitz, B., Robock, A., Shindell, D. T., Miller, M. A., 2012. Sensitivity of stratospheric geoengineering with black carbon to aerosol size and altitude of injection. Journal of Geophysical Research: Atmospheres 117 (D9), n/a–n/a, d09203.
URL http://dx.doi.org/10.1029/2011JD017341

Krittaya, L., 2007. Flame at ptt, map ta phut, rayong, thailand. File: Flame_at_PTT_map_ta_phut.jpg, Public domain.
URL https://commons.wikimedia.org/wiki/File:PTT_flame_1.jpg

Kuijpers, K. R., de Martn, L., van Ommen, J. R., 2014. Optimizing off-lattice diffusion-limited aggregation. Computer Physics Communications 185 (3), 841 – 846.
URL http://www.sciencedirect.com/science/article/pii/S0010465513004153

Kylling, A., 2016. Radiative forcing, unpublished report.

Lévy, P., Borel, M. É., 1954. Théorie de l'addition des variables aléatoires. Vol. 1. Gauthier-Villars Paris.

Li, X., Maring, H., Savoie, D., Voss, K., Prospero, J. M., 04 1996. Dominance of mineral dust in aerosol light-scattering in the north atlantic trade winds. Nature 380 (6573), 416–419.
URL http://dx.doi.org/10.1038/380416a0

Lide, D., 2004. CRC Handbook of Chemistry and Physics, 85th Edition. No. Bd. 85 in CRC Handbook of Chemistry and Physics, 85th Ed. Taylor & Francis.
URL https://books.google.de/books?id=WDll8hA006AC

Liousse, C., Cachier, H., Jennings, S., 1993. Optical and thermal measurements of black carbon aerosol content in different environments: Variation of the specific attenuation cross-section, sigma (). Atmospheric Environment. Part A. General Topics 27 (8), 1203 – 1211.
URL http://www.sciencedirect.com/science/article/pii/096016869390246U

Mandelbrot, B. B., 1975. Stochastic models for the earth's relief, the shape and the fractal dimension of the coastlines, and the number-area rule for islands. Proceedings of the National Academy of Sciences 72 (10), 3825–3828.
URL http://www.pnas.org/content/72/10/3825.abstract

Maring, H., Savoie, D. L., Izaguirre, M. A., Custals, L., Reid, J. S., 2003. Mineral dust aerosol size distribution change during atmospheric transport. Journal of Geophysical Research: Atmospheres 108 (D19), n/a–n/a, 8592.
URL http://dx.doi.org/10.1029/2002JD002536

Marks, A., King, M., 2013. The effects of additional black carbon on the albedo of arctic sea ice: variation with sea ice type and snow cover. The Cryosphere 7 (4), 1193–1204.

Marticorena, B., Chatenet, B., Rajot, J. L., Traoré, S., Coulibaly, M., Diallo, A., Koné, I., Maman, A., NDiaye, T., Zakou, A., 2010. Temporal variability of mineral dust concentrations over west africa: analyses of a pluriannual monitoring from the amma sahelian dust transect. Atmospheric Chemistry and Physics 10 (18), 8899–8915.
URL http://www.atmos-chem-phys.net/10/8899/2010/

Mayer, B., Kylling, A., 2005. Technical note: The libradtran software package for radiative transfer calculations - description and examples of use. Atmospheric Chemistry and Physics 5 (7), 1855–1877.
URL http://www.atmos-chem-phys.net/5/1855/2005/

Meakin, P., Sep 1983. Formation of fractal clusters and networks by irreversible diffusion-limited aggregation. Phys. Rev. Lett. 51, 1119–1122.
URL http://link.aps.org/doi/10.1103/PhysRevLett.51.1119

Meakin, P., Vicsek, T., Family, F., Jan 1985. Dynamic cluster-size distribution in cluster-cluster aggregation: Effects of cluster diffusivity. Phys. Rev. B 31, 564–569.
URL http://link.aps.org/doi/10.1103/PhysRevB.31.564

Meneveau, C., Sreenivasan, K. R., Sep 1987. Simple multifractal cascade model for fully developed turbulence. Phys. Rev. Lett. 59, 1424–1427.
URL http://link.aps.org/doi/10.1103/PhysRevLett.59.1424

Menut, L., Forłt, G., Bergametti, G., 2007. Sensitivity of mineral dust concentrations to the model size distribution accuracy. Journal of Geophysical Research: Atmospheres 112 (D10), n/a–n/a, d10210.
URL http://dx.doi.org/10.1029/2006JD007766

Richardson, L. F., 1922. Weather Prediction by Numerical Process, 1st Edition. Cambridge University Press.
URL https://archive.org/details/weatherpredictio00richrich

Rosen, J. M., 1964. The vertical distribution of dust to 30 kilometers. Journal of Geophysical Research 69 (21), 4673–4676.
URL http://dx.doi.org/10.1029/JZ069i021p04673

Ryder, C. L., Highwood, E. J., Rosenberg, P. D., Trembath, J., Brooke, J. K., Bart, M., Dean, A., Crosier, J., Dorsey, J., Brindley, H., Banks, J., Marsham, J. H., McQuaid, J. B., Sodemann, H., Washington, R., 2013. Optical properties of saharan dust aerosol and contribution from the coarse mode as measured during the fennec 2011 aircraft campaign. Atmospheric Chemistry and Physics 13 (1), 303–325.
URL http://www.atmos-chem-phys.net/13/303/2013/

Sand, M., Berntsen, T. K., von Salzen, K., Flanner, M. G., Langner, J., Victor, D. G., Nov 2015. Response of arctic temperature to changes in emissions of short-lived climate forcers. Nature Clim. Change advance online publication.
URL http://dx.doi.org/10.1038/nclimate2880

Scarnato, B. V., China, S., Nielsen, K., Mazzoleni, C., 2015. Perturbations of the optical properties of mineral dust particles by mixing with black carbon: a numerical simulation study. Atmospheric Chemistry and Physics Discussions 15 (2), 2487–2533.
URL http://www.atmos-chem-phys-discuss.net/15/2487/2015/

Schertzer, D., Lovejoy, S., Hubert, P., April 2008. An introduction to stochastic multifractal fields.
URL http://www.physics.mcgill.ca/~gang/eprints/eprintLovejoy/DS_stoch.multif0801.pdf

Schwartz, J., Neas, L. M., 2000. Fine particles are more strongly associated than coarse particles with acute respiratory health effects in schoolchildren.
URL http://journals.lww.com/epidem/Fulltext/2000/01000/Fine_Particles_Are_More_Strongly_Associated_than.4.aspx

Seinfeld, J. H., 1986. Atmospheric chemistry and physics of air pollution. Wiley, New York.

Shlesinger, M. F., West, B. J., Klafter, J., Mar 1987. Lévy dynamics of enhanced diffusion: Application to turbulence. Phys. Rev. Lett. 58, 1100–1103.
URL http://link.aps.org/doi/10.1103/PhysRevLett.58.1100

Sokolik, I. N., Toon, O. B., 06 1996. Direct radiative forcing by anthropogenic airborne mineral aerosols. Nature 381 (6584), 681–683.
URL http://dx.doi.org/10.1038/381681a0

Stamnes, K., Tsay, S.-C., Wiscombe, W., Jayaweera, K., Jun 1988. Numerically stable algorithm for discrete-ordinate-method radiative transfer in multiple scattering and emitting layered media. Appl. Opt. 27 (12), 2502–2509.
URL http://ao.osa.org/abstract.cfm?URI=ao-27-12-2502

Stocker, T. F., 2014. Climate change 2013: the physical science basis: Working Group I contribution to the Fifth assessment report of the Intergovernmental Panel on Climate Change. Cambridge University Press.

Strogatz, S., 1994. Nonlinear Dynamics and Chaos: With Applications to Physics, Biology, Chemistry, and Engineering. Advanced book program. Westview Press.
URL https://books.google.no/books?id=FIYHiBLWCJMC

Tegen, I., Fung, I., 1994. Modeling of mineral dust in the atmosphere: Sources, transport, and optical thickness. Journal of Geophysical Research: Atmospheres 99 (D11), 22897–22914.
URL http://dx.doi.org/10.1029/94JD01928

Tikhomirov, V. M., 1991a. Selected Works of A. N. Kolmogorov: Volume I: Mathematics and Mechanics. Springer Netherlands, Dordrecht, Ch. Local Structure Of Turbulence in an Incompressible Viscous Fluid at Very Large Reynolds Numbers, pp. 312–318.
URL http://dx.doi.org/10.1007/978-94-011-3030-1_45

Tikhomirov, V. M., 1991b. Selected Works of A. N. Kolmogorov: Volume I: Mathematics and Mechanics. Springer Netherlands, Dordrecht, Ch. On the Degeneration of Isotropic Turbulence in an Incompressible Viscous Fluid, pp. 319–323.
URL http://dx.doi.org/10.1007/978-94-011-3030-1_46

Vicsek, T., Family, F., May 1984. Dynamic scaling for aggregation of clusters. Phys. Rev. Lett. 52, 1669–1672.
URL http://link.aps.org/doi/10.1103/PhysRevLett.52.1669

Witten, T. A., Sander, L. M., Nov 1981. Diffusion-limited aggregation, a kinetic critical phenomenon. Phys. Rev. Lett. 47, 1400–1403.
URL http://link.aps.org/doi/10.1103/PhysRevLett.47.1400

Yaglom, A. M., Jul. 1966. The Influence of Fluctuations in Energy Dissipation on the Shape of Turbulence Characteristics in the Inertial Interval. Soviet Physics Doklady 11, 26.